

Investigation of the Electrical, Thermal and Mechanical Properties of Graphene Reinforced Low Density Polyethylene Nanocomposite

*A dissertation submitted to the Department of Physics, Bangladesh University of
Engineering and Technology, Dhaka in partial fulfillment of the requirements
for the degree of MASTER OF SCIENCE (M.Sc.) IN PHYSICS*

by

Md. Mehedi Hasan Sohag

MASTER OF SCIENCE (M.Sc.) IN PHYSICS

Department of Physics

Roll No. 0417142523F

Session: April, 2017

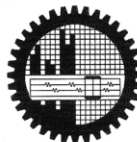


BANGLADESH UNIVERSITY OF ENGINEERING AND TECHNOLOGY

BUET, Dhaka-1000

December, 2019

UNIVERSITY OF ENGINEERING & TECHNOLOGY (BUET), DHAKA
DEPARTMENT OF PHYSICS



Certification of Thesis

The thesis titled “**INVESTIGATION OF THE ELECTRICAL, THERMAL AND MECHANICAL PROPERTIES OF GRAPHENE REINFORCED LOW DENSITY POLYETHYLENE NANOCOMPOSITE**” submitted by **Md. Mehedi Hasan Sohag**, Roll No. 0417142523F, Session: April/2017, has been accepted as satisfactory in partial fulfillment of the requirement for the degree of **Masters of Science (M.Sc.)** in Physics on 11 December, 2019.

BOARD OF EXAMINERS

Dr. Mohammad Jellur Rahman
(Supervisor)
Associate Professor
Department of Physics, BUET, Dhaka

Chairman

Dr. Md. Forhad Mina
Professor and Head
Department of Physics, BUET, Dhaka-1000

Member (Ex-Officio)

Dr. Mohammed Abdul Basith
Professor
Department of Physics, BUET, Dhaka-1000

Member

Dr. Parvin Sultana
Assistant Professor
Department of Physics, BUET, Dhaka-1000

Member

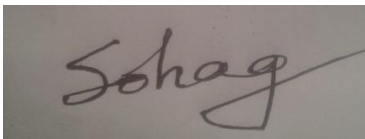
Dr. Md. Abdul Gafur
Principal Scientific Officer
Institute of Fuel Research and Development (IFRD)
BCSIR, Dhaka-1205

Member (External)

CANDIDATE'S DECLARATION

It is hereby declared that this thesis or any part of it has not been submitted elsewhere for the award of any degree or diploma.

Signature of the candidate

A rectangular box containing a handwritten signature in black ink. The signature is written in a cursive style and appears to read 'Sohag'.

(Md. Mehedi Hasan Sohag)

Roll No. 0417142523F

Session: April, 2017

Dedicated
To
My Dear Parents and Teachers

CONTENTS	Page No.
CANDIDATE’S DECLARATION	iii
DEDICATION	iv
LIST OF FIGURES	ix–xi
LIST OF TABLES	xii
LIST OF ABBREVIATIONS	xiii
ACKNOWLEDGEMENTS	xiv
ABSTRACT	v

CHAPTER 1

GENERAL INTRODUCTION	(01–08)
1.1 Introduction	01
1.2 Nanotechnology	02
1.3 Nanocomposites	03
1.4 Polymer Based Nanocomposite	03
1.5 Literature Review	04
1.6 Objectives of this Study	07
1.7 Outline of this Thesis	08

CHAPTER 2

THEORITICAL BACKGROUND	(09–31)
2.1 Polymers	09
2.1.1 Natural polymers	10
2.1.2 Synthetic polymers	10
2.2 Polyethylene	10

2.2.1	High density polyethylene (HDPE)	11
2.2.2	Low density polyethylene (LDPE)	11
2.3	Graphene	12
2.4	Nanocomposite Synthesis Techniques	13
2.4.1	Molding method/technique	13
2.4.1.1	Extrusion molding	13
2.5	Extrusion Molding Machine (EMM)	14
2.5.1	The screw design	16
2.5.2	The screw variable	17
2.5.3	Operation of EMM	18
2.5.4	Advantages/disadvantages of EMM	19
2.6	Surface Morphology	19
2.6.1	Scanning electron microscopy (SEM)	19
2.6.2	Transmission electron microscopy (TEM)	20
2.7	Elemental Analysis	21
2.7.1	Energy dispersive x-ray (EDX) spectroscopy	21
2.8	Structural Analyses	23
2.8.1	X-Ray diffraction (XRD)	23
2.8.2	Fourier transform infrared (FTIR) spectroscopy	24
2.9	Thermal Analyses	25
2.9.1	Thermogravimetric/derivative thermogravimetric (TG/DTG) analysis	25
2.10	Mechanical Strength	27
2.10.1	Tensile strength	27
2.11	Electrical Properties	28
2.11.1	Conductivity measurements setup	29
2.11.2	Current Density	30
2.11.3	DC Electrical conductivity	30
2.11.4	Activation energy	31
2.11.5	Dielectric properties	31

CHAPTER 3

EXPERIMENTAL DETAILS

(33–44)

3.1	Materials	33
3.2	Apparatus Used For This Work	33
3.2.1	Analytical balance meter	33
3.2.2	Hot plate magnetic stirrer	34
3.2.3	Ultrasonic bath	34
3.2.4	Centrifuge machine	34
3.2.5	Universal hot air oven	35
3.3	Fabrication of Extrusion Molding (EMM)	35
3.4	Composite Fabrication	36
3.4.1	RGO synthesis	36
3.4.2	RGO/LDPE nanocomposite	38
3.5	Characterization of the Composites	39
3.5.1	Surface morphology	39
3.5.2	Elemental analysis	39
3.5.3	Structural analysis	40
3.5.3.1	X–ray diffraction (XRD)	40
3.5.3.2	Fourier transform infrared (FTIR) spectroscopy	40
3.5.4	Thermal stability	41
3.5.5	Mechanical strength	42
3.5.6	Electrical conductivity	43
3.5.6.1	DC electrical measurement	43
3.5.6.2	AC electrical measurement	44

CHAPTER 4

RESULTS AND DISCUSSION

(45–69)

4.1	Surface Morphology	45
4.1.1	Surface morphology of RGO and RGO/LDPE nanocomposite	45
4.2	Elemental Analysis	50

4.2.1	Energy Dispersive X-ray Analysis (EDX)	50
4.3	Structural Analyses	54
4.3.1	X-ray diffraction (XRD) pattern	54
4.3.2	Fourier transform infrared (FTIR) spectroscopy	56
4.4	Thermal Analyses	58
4.4.1	Thermogravimetric/derivative thermogravimetric (TG/DTG) analysis	58
4.5	Mechanical Strength	59
4.6	Electrical Properties	61
4.6.1	DC current density	61
4.6.2	DC electrical conductivity	65
4.6.3	Dielectric properties	66

CHAPTER 5

CONCLUSIONS (70–81)

5.1	Conclusions	70
5.2	Recommendations for Future Work	72
5.3	References	73

LIST OF FIGURES

Fig. No.		Page No.
1.1	Comparison of nanomaterial sizes.	2
1.2	XRD image of (a) RGO1 and (b) RGO2.	4
1.3	XRD image of graphene, LDPE and graphene/LDPE nanocomposite.	5
1.4	SEM images of (a) graphene and (b) graphene/LDPE nanocomposite.	6
1.5	(a) TGA curve and (b) frequency dependent electrical conductivity of pure LDPE and RGO-AO/LDPE nanocomposite.	6
1.6	Stress-strain curve for pure LDPE and graphene/LDPE nanocomposite.	7
2.1	Block diagram of branching of LDPE.	11
2.2	A block diagram of Extrusion Molding Machine (EMM).	15
2.3	A block diagram of single screw extruder design.	16
2.4	Schematic diagram of a FESEM machine.	20
2.5	Schematic diagram of a TEM machine.	21
2.6	Schematic diagram of X-rays production.	22
2.7	Schematic diagram of Bragg's XRD equation.	23
2.8	Schematic diagram of FTIR.	24
2.9	Schematic diagram of TG/DTG analyzer.	26
2.10	Tensile strength measurement setup.	28
2.11	Two probe method circuit diagram.	29
3.1	Analytical Balance Meter (Left) and Hot plate magnetic stirrer (Right).	33
3.2	Photograph of Ultrasonic bath (Left) and centrifuge machine (Right).	34
3.3	A photograph of universal hot air oven.	35
3.4	Extrusion Molding Machine (EMM) set up.	36
3.5	Flowchart of GO and RGO synthesis.	37
3.6	RGO/LDPE nanocomposite preparation flowchart.	38
3.7	Field emission scanning electron microscope (FESEM) set up.	39
3.8	X-ray diffractometer set up.	40

3.9	A photograph of FTIR setup.	41
3.10	A TG/DTG measuring setup.	42
3.11	A photograph of tensile strength measurement setup.	43
3.12	DC electrical measurement set up.	43
3.13	AC electrical measurement set up.	44
4.1	FESEM images of RGO at (a) $\times 3k$ and (b) $\times 30k$ magnification.	45
4.2	FESEM images of pure LDPE at (a) $\times 3k$ and (b) $\times 30k$ magnification.	46
4.3	FESEM images of 1.0 wt% RGO/LDPE nanocomposite at (a) $\times 3k$ and (b) $\times 30k$ magnification.	47
4.4	FESEM images of 2.0 wt% RGO/LDPE nanocomposite at (a) $\times 3k$ and (b) $\times 30k$ magnification.	48
4.5	FESEM images of 3.0 wt% RGO/LDPE nanocomposite at (a) $\times 3k$ and (b) $\times 30k$ magnification.	49
4.6	EDX spectra of (a) RGO and (b) 0.0 wt% RGO loaded RGO/LDPE nanocomposites.	51
4.7	EDX spectra of (a) 1.0 wt% and (b) 2.0 wt% RGO loaded RGO/LDPE nanocomposites.	52
4.8	EDX spectra of 3.0 wt% RGO loaded RGO/LDPE nanocomposite.	53
4.9	XRD patterns of RGO.	54
4.10	XRD patterns of (a) RGO and (b–e) RGO loaded RGO/LDPE nanocomposite.	55
4.11	FTIR spectra of pure LDPE and RGO loaded RGO/LDPE composite.	57
4.12	(a) TG/DTG curves of pure LDPE and RGO loaded RGO/LDPE nanocomposites and (b) Highlight of T_{onset} .	58
4.13	Stress–strain curves for pure LDPE and RGO loaded RGO/ LDPE nanocomposite.	60
4.14	J–V characteristic curves of pure LDPE at different temperature.	61
4.15	J–V characteristic curves of (a) 1.0 wt% and (b) 2.0 wt% of RGO loaded RGO/LDPE nanocomposite at different temperature.	62

4.16	J–V characteristic curves of 3.0 wt% of RGO loaded RGO/LDPE nanocomposite at different temperature.	63
4.17	J–V characteristic curves of RGO loaded RGO/LDPE nanocomposite at temperature (a) 303 K and (b) 333 K.	64
4.18	J–V characteristic curves of RGO loaded RGO/LDPE nanocomposite at temperature 363 K.	65
4.19	DC conductivity with respect to different wt% of RGO in RGO loaded RGO/LDPE nanocomposite at different temperature.	66
4.20	Graphical representation of frequency dependent (a) dielectric constant and (b) dielectric loss.	67
4.21	Graphical representation of frequency dependent electrical conductivity.	68

LIST OF TABLES

Table No.		Page No.
4.1	Elemental analysis data of RGO and different wt% of RGO in the RGO/LDPE nanocomposite.	53
4.2	XRD measurement data of RGO and RGO loaded RGO/LDPE nanocomposite.	56
4.3	TGA measurement data of pure LDPE and RGO/LDPE nanocomposite.	59
4.4	Mechanical testing data of RGO/LDPE nanocomposites.	60

LIST OF ABBREVIATIONS

EMM	Extrusion molding machine
RGO	Reduced graphene oxide
LDPE	Low density polyethylene
HDPE	High density polyethylene
λ	Wavelength
θ	Bragg angle
k_B	Boltzmann constant
ΔE	Activation energy
σ	Electrical conductivity
J	Current density
ρ	Resistivity
D	Crystallite size
β	Full width half maximum
R	Electrical resistance
T	Temperature

ACKNOWLEDGEMENTS

First of all, I am eternally grateful to the almighty creator Allah who has given me the opportunity and strength to complete the thesis properly.

I would like to express massive gratitude to my respected supervisor Dr. Mohammad Jellur Rahman, Associate Professor, Department of Physics, BUET, for his guidelines and unconditional support that helps to proceed with my higher study. I am also grateful to him for suggesting me to research about the emergent field of polymer nanocomposite.

I am decently grateful to Professor Dr. Md. Forhad Mina, Head, Department of Physics, BUET, for providing splendid research facilities in the Department.

I am humbly thankful to Professor Dr. Md. Abu Hashan Bhuiyan for encouraging me to keep strength for a long time patiently throughout the research work.

I am very much indebted to Dr. Mohammad Abdul Basith, Dr. Muhammad Rakibul Islam, Dr. Parvin Sultana as well as all of my respected teachers of the Department of Physics, BUET for their innumerable suggestions and inspirations.

I would like to give jubilant and convincing thanks to all of my dear current and former members of the Material Science and Polymer Nanocomposite Lab., Department of Physics, BUET, for their amiable deeds.

I would also like to express the vast gratitude to Dr. Md. Abdul Gafur, Principal Scientific Officer, Institute of Fuel Research and Development (IFRD), BCSIR, Dhaka for allowing me in his Lab to characterize the material.

I am also acknowledged to the Department of Chemistry, Department of Glass and Ceramic Engineering, Department of Biomedical Engineering, BUET for allowing me to use their Lab for sample characterization.

I am also thankful to the Committee for Advanced Studies and Research (CASR), BUET for providing financial support to do this thesis work.

I am very much thankful to all the staff of the Department of Physics, BUET for their satisfactory assistance.

I am also very much grateful to all of my family members for their unconditional support to pursue my higher study.

Md. Mehedi Hasan Sohag

December, 2019

ABSTRACT

Low-density polyethylene (LDPE), the synthetic polymer is widely used material due to its excellent properties and applications such as, in the automobile industry, the insulator of electric wire, laboratory equipment, etc. In spite of a large number of applications, the LDPE has some limitations in electrical, mechanical and thermal applications, thus to overcome these limitations it needs to be incorporated with other filler materials. Several materials are used as fillers, among them graphene, the derivative of carbon is widely used filler owing to its redundant performance in modern technology. The newly invented 2D wonder material graphene has auspicious presentation because of its lightweight, very strong and high mobility for charge carriers. The graphene is synthesized from natural graphite powder by chemical reduction method. Having synthesized the graphene is added to the LDPE matrix. Many composite fabrication techniques are available, among them, the extrusion molding method is best to avoid the problematic functionalization of graphene. The machine used for this techniques is called the extrusion molding machine (EMM). In this machine, the composites are fabricated by the simultaneous operation of heater and extruder. The EMM is locally fabricated where the necessary components are collected from a local market at a very low cost. Then the graphene reinforced LDPE nanocomposites are prepared by using this machine. The fabricated nanocomposites are studied by field emission scanning electron microscopy (FESEM) analysis to obtain surface morphology. This result reveals that the filler contents are properly dispersed in the matrix. Structural analysis is investigated by x-ray diffraction (XRD). The chemical structure is studied by Fourier transform infrared (FTIR) spectroscopy. Thermal stability is investigated by thermogravimetric analysis (TGA), which is very consistent with the theoretical value. Mechanical strength is observed by the calculation of ultimate tensile strength (UTS) and Young modulus. Current density, electrical conductivity, and dielectric constant are investigated to obtain the electrical properties of the as-synthesized nanocomposites. The current density is increased with increasing temperature, which is very consistent with the semiconducting nature of material.

CHAPTER 1

GENERAL INTRODUCTION

1.1 Introduction

Nowadays modern science and technology is largely dependent on materials. Material scientists and engineers have been working for several decades to investigate the intangible properties of material. In the modern era the application of materials are beyond description. Even the world's most attractive lightweight vehicles are the royal application of these materials [1]. Several types of material is being used to our demand like as–

- Engineering material
- Advance material
- Smart material
- Polymer material
- Metal material
- Ceramic material
- Nanomaterial

Among them polymers are broadly used materials around us. Polymers are generally two types such as, natural and synthetic polymer. Low density polyethylene (LDPE) is a synthetic polymer which is abundantly used in the household and industry as different types of vessel and insulating material [2]. Despite of this versatile applications, the LDPE has some limitations in electrical, mechanical and thermal applications. The main aim of this thesis is to investigate different properties of pure LDPE by incorporating with a filler agent and try to overcome these limitations. Reduced graphene oxide (RGO), a derivative of graphene is chosen here as filler agent for the groundbreaking applications in every sector of science and technology. Extrusion molding, a method of fabricating material is selected for this experiment to avoid the functionalization of RGO. The machine used for this process is known as extrusion molding machine (EMM) is fabricated locally. Best efforts have been given for proper mixing of the composite but the polymer nanocomposite has a little bit limitations in proper dispersion unlike metal nanocomposite due to the non-polar behavior of polymer.

1.2 Nanotechnology

The term ‘nano’ comes from the Greek word ‘nanos’ which means dwarfs. The term nanotechnology and nanoscience is closely related with the ‘nano scale’ range material. The nanometer is one billionth of a meter. Nanotechnology is the application of extremely small material that can be used to all other science and technology. The material of size about 1 to 100 nm is called nanomaterial. The comparison of nanomaterial sizes are as given below:

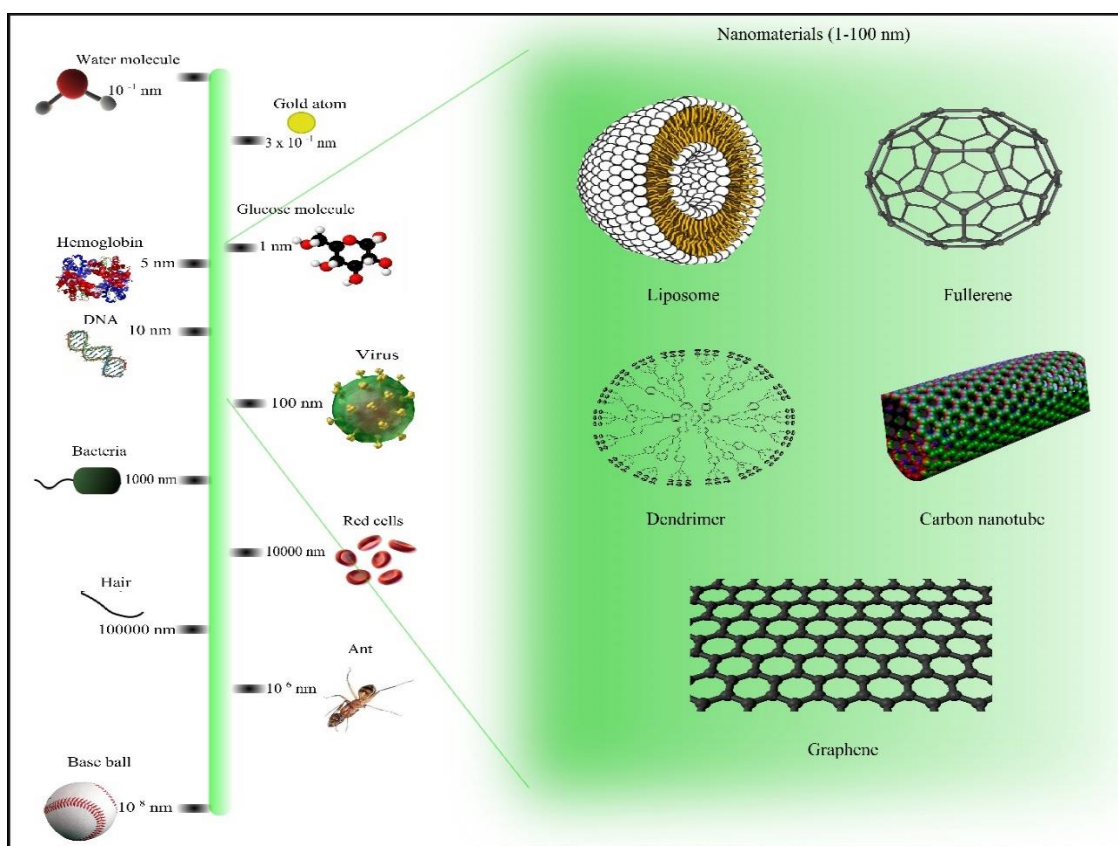


Figure 1.1: Comparison of nanomaterial sizes. (Source: Wikipedia).

The details idea about nanotechnology came from the talk, “There's a plenty of room at the bottom” given by the Nobel laureate physicist Richard P. Feynman at annual meeting of American Physical Society (APS) at the California Institute of Technology (CalTech) on December 29, 1959 [3]. The groundbreaking applications of nanotechnology have already changed the world by manipulating different experimental techniques. The outcome of the nanotechnology can be seen in different sectors such as,

- Nanotechnology in electronics
- Nanotechnology in energy
- Nanotechnology in material
- Nanotechnology in manufacturing
- Nanotechnology in medicine

1.3 Nanocomposites

Nanocomposites are the composite material having at least one of the phases with dimension in nanometer range. These are the materials in which nanosized filler components are added to other materials in order to change the properties of the resulting materials. The properties of composite material is different from any of the constituents. The constituent materials that is in greater quantity is called the matrix and the constituent in small quantity is called filler agents. Basically the choice of filler depends on the demand of our applications. The polymer matrix and fillers are generally bonded by weak intermolecular forces. In order to achieve the improve properties of nanocomposites, the fillers should be dispersed and distributed to the matrix properly, otherwise the properties of nanocomposites will be reduced by introducing agglomeration. A good dispersion of nanomaterial is hard to achieve in non-polar material. Filler agents are generally in the form of nanosized thus it is called nanomaterial and the resultant material is called nanocomposite. According to the types of filler and matrix nanocomposites are classified into following classes [4]:

- Polymer based nanocomposites
- Ceramic based nanocomposites
- Metal based nanocomposites
- Carbon based nanocomposites
- Cement based nanocomposites

1.4 Polyethylene Based Nanocomposites

Polyethylene, the synthetic polymer is widely used as matrix in nanocomposite. The polyethylene has been using in multiple sectors of material science and engineering but it has some limitation in electrical, mechanical and thermal applications. Thus in order to

overcome these limitations the filler/nanofiller materials should be added and hence the resultant material is called polyethylene based nanocomposite. The polyethylene based nanocomposites have attracted fruitful attention to material scientist due to their remaining mechanical and thermal properties [5]. After mixing with additives the new materials' degradation temperature is higher rather than the pure, thus these can be used in industry as a highly thermal insulative material. Moreover the tensile strength of the new material is high thus, these can be used in automobile and sports manufacturing industry.

1.5 Literature Review

Bhavana et al. [6] have synthesized the RGO in two steps named as RGO1 and RGO2 (Fig. 1.2). The hydroxyl (RGO1) and epoxy-hydroxyl (RGO2) functionalized RGO samples were prepared by chemical reduction method. Two XRD peaks of the two curves are observed at 21.5° and 24.8° in the plane (002) of the interlayer spacing of 0.4 and 0.36 nm, respectively. They also explained that the broad peak represents few layers of RGO sheets and interlayer spacing is decreased due to the removal of oxygen functional groups.

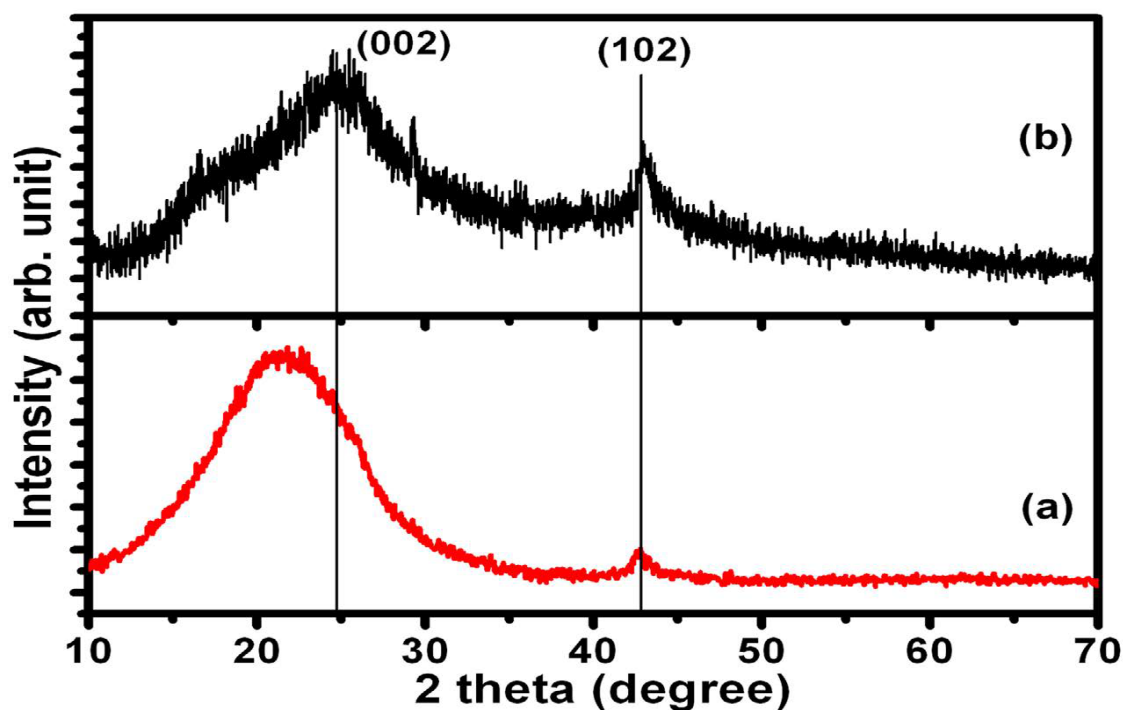


Figure 1.2: XRD image of (a) RGO1 and (b) RGO2.

Sabet et al. [7] have observed graphene/LDPE nanocomposite where twin screw mixer and hot press casting method was used to fabricate and shape. A broad peak of graphene at 26° and two peaks at 20.96° , 23.21° of graphene/LDPE nanocomposite were observed (Fig. 1.3). They have also explained that the crystallite size of the nanocomposites are increased by the inclusion of graphene in LDPE.

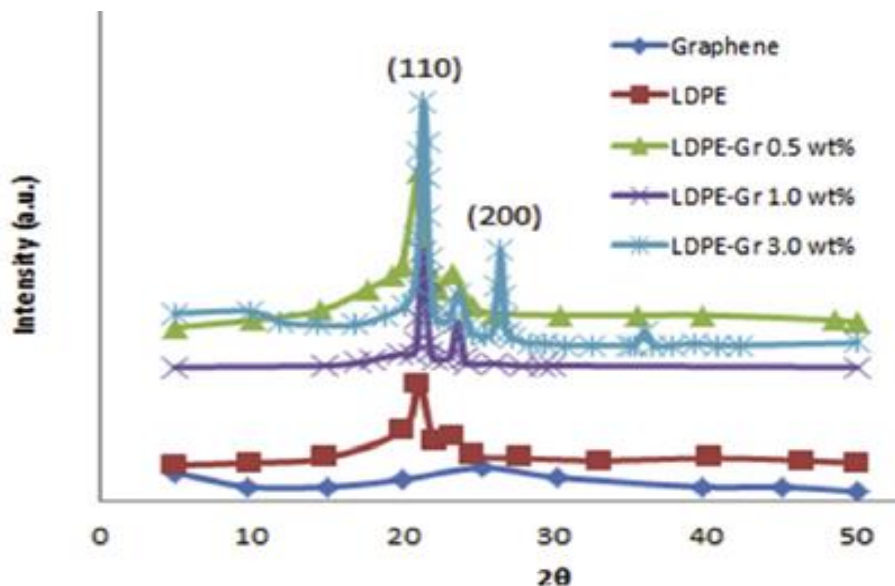


Figure 1.3: XRD image of graphene, LDPE and graphene/LDPE nanocomposite.

The same authors [7] have also explained the surface morphology of the nanocomposite and observed that the SEM photograph of graphene (Fig. 1.4a) shows maximum exfoliation at 1000°C . The appearance of island like regions in the composites (Fig. 1.4b) with relatively higher loading of graphene indicates the dispersion of graphene in the LDPE by showing highly wrinkled structure. The certain surface promotes a decrease in agglomeration and increases in interactions between graphene and LDPE.

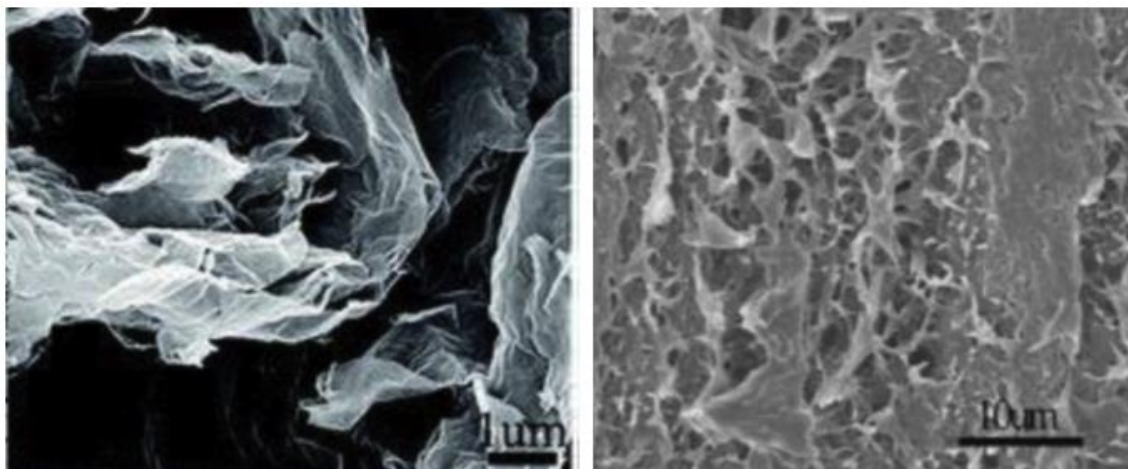


Figure 1.4: SEM images of (a) graphene and (b) graphene/LDPE nanocomposite.

Jing et al. [8] studied the RGO-AO (antioxidant) /LDPE nanocomposite by solution casting process and investigated their performance in thermal analysis (Fig. 1.5a). They explained that the initial degradation temperature of pure LDPE is relatively low and it is increased with the increase of RGO-AO loading. They also observed the frequency dependent electrical conductivity (Fig. 1.5b) and explained that the conductivity is dependent on frequency and the results give another information that the electrical insulation level increased by the addition of RGO-AO. The addition of RGO-AO introduced deep traps in composites which decreases the free charge carriers hence electrical conductivity is decreased by the addition of RGO-AO in pure LDPE.

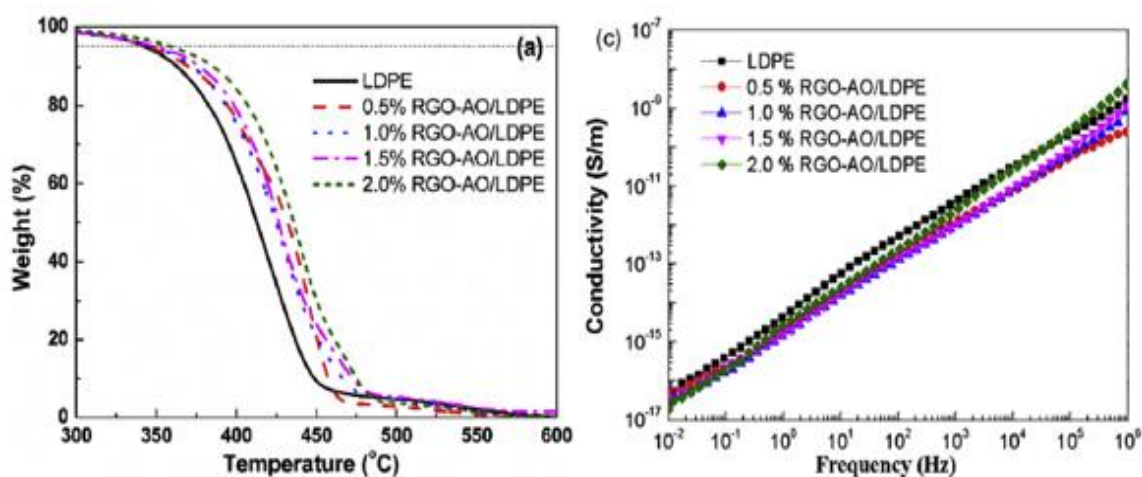


Figure 1.5: (a) TGA curve and (b) frequency dependent electrical conductivity of pure LDPE and RGO-AO/LDPE nanocomposite.

Irene et al. [9] studied graphene/LDPE nanocomposite manufactured by mechanical mixing (Turbula mixer machine) method and observed the mechanical properties (Fig. 1.6). The stress-strain graph shows the tensile strength is increased with the increase of graphene concentration. They also added that the tensile strength is increased by 70% rather than pure LDPE.

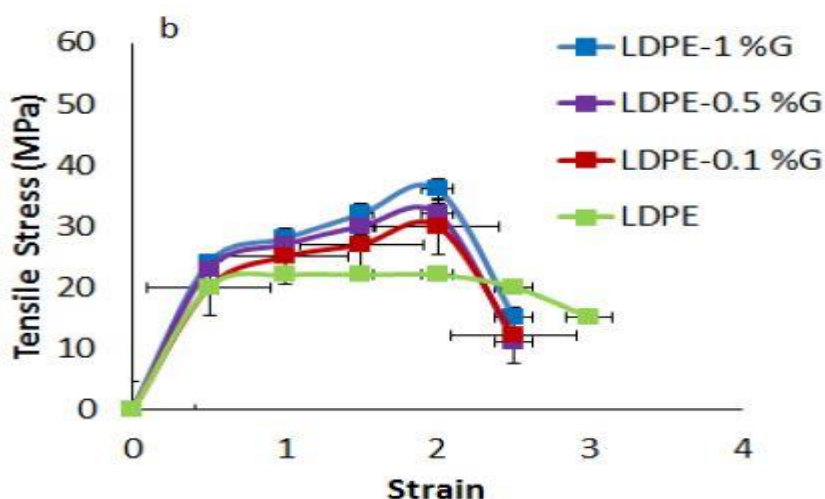


Figure 1.6: Stress-strain curve for pure LDPE and graphene/LDPE nanocomposite.

1.6 Objectives of this Study

The aim and objectives of this thesis is to investigate different physical and chemical properties of reduced graphene oxide (RGO) reinforced low density polyethylene (LDPE). RGO, the derivative of carbon has fruitful electrical, mechanical and thermal properties. On the other hand LDPE is a synthetic polymer of insulating properties. The RGO/LDPE nanocomposite will be used in technology and textile industry for advance applications. The notable objectives of this thesis is given below:

- To fabricate an extrusion molding machine (EMM) for composite preparation.
- To synthesis reduced graphene oxide (RGO) using Hummers' method and prepare RGO/LDPE nanocomposites by using EMM.
- To investigate the crystallite size and surface morphology of the pure LDPE and LDPE/RGO nanocomposites by using X-ray diffraction (XRD) and field emission scanning electron microscopy (FESEM) analysis, respectively.

- To investigate the chemical bonding structure of the composite by using Fourier transform infrared spectroscopy (FTIR).
- To study the ac and dc electrical properties.
- To observe the thermal stability by thermogravimetric (TG) and derivative thermogravimetric (DTG) analysis.
- To investigate the mechanical properties of the nanocomposites and to compare with the pure matrix.

1.7 Outline of this Thesis

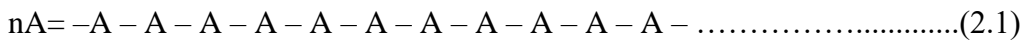
- Chapter 1 describes a general introduction and literature review.
- Chapter 2 describes about polymer, polyethylene, nanocomposite synthesis techniques, extrusion molding machine, etc.
- Chapter 3 describes about the experimental setup, composite fabrication techniques and characterization.
- Chapter 4 describes the results and discussion of this research work.
- Chapter 5 includes conclusions and suggestions for future work and references.

CHAPTER 2

THEORETICAL BACKGROUND

2.1 Polymers

The term 'polymer' was originated from the Greek word 'poly' which means many and 'mer' means part, defining a macromolecule. A polymer is a long-chain molecule that is composed of a large number of repeating small molecules of indistinguishable structure known as monomer and the process is called polymerization. The polymers have a large number of applications in daily life due to their jubilant properties [10]. Because of their large number of superficial applications the polymer have already been attracted a great attention in the field of biophysics, material sciences, nanotechnology, etc. Polymers can be considered as the bonding of a large number of monomers which can be shown by a general equation:



Where 'n' is the number of monomer (A).

However the polymers are numerous in number and is found in naturally or artificially that can be classified in different ways as follows [11]:

- (i) Classification based on source
 - (a) Natural Polymer
 - (b) Synthetic Polymer
- (ii) Classification based on structure of polymer
 - (a) Linear Polymer
 - (b) Branched Polymer
 - (c) Cross-linked or network polymer
- (iii) Classification based on mode of polymerization
 - (a) Addition Polymer
 - (b) Condensation Polymer
- (iv) Classification based on molecular forces
 - (a) Elastomer
 - (b) Thermoplastics
 - (c) Thermosetting

2.1.1 Natural polymers

The polymers which are available in nature and can be extracted from animals and plants are known as natural polymer. The common example of natural polymers are: proteins, starch, cellulose, rubber, etc.

2.1.2 Synthetic polymers

The most available and cheap polymers are synthetic polymers. The polymers which are artificially synthesized by human in a laboratory at specific requirements are known as synthetic polymers. It has a large number of applications in daily life. Several industries have been built around synthetic polymer which has redundantly changed the scenario of mills and industries. The common types of synthetic polymers are:

- Polyethylene (PE)
- Polypropylene (PP)
- Polyvinyl Alcohol (PVA)
- Polyvinyl Chloride (PVC)
- Polystyrene (PS)
- Nylon (Nylon 6, Nylon 6,6)
- Teflon (Polytetrafluoroethylene)
- Thermoplastic polyurethanes (TPU), etc.

2.2 Polyethylene

Polyethylene is one of the most widely used thermoplastic polymer which is formed of ethylene monomer. It is the most common plastic used in household and industries. Its primary use is in packaging like as plastic bags, bottles, containers, pipes, cover of electric wire etc. It is very familiar plastic due to low cost, excellent dielectric properties, moisture resistance, and very good chemical resistance. Different types of polyethylene are available around us, among them the two notable type's types:

- a) High density polyethylene (HDPE)
- b) Low density polyethylene (LDPE)

2.2.1 High density polyethylene (HDPE)

HDPE is defined by its density ($930\text{--}970\text{ kg/m}^3$) and mechanical strength which are greater than those of other polyethylene. It has a low degree of branching, so intermolecular forces are stronger than in highly branched polymers. HDPE is normally found in shopping bags and kitchen tidy bags, pipes, tanks, etc. It is also used to make plastic furniture, insulator of electric wires, etc. It is slightly harder and stiffer than other polyethylene, it feels rough to touch, and has an opaque appearance.

2.2.2 Low density polyethylene (LDPE)

LDPE, the thermoplastic polymer is made of ethylene monomer. Its density is comparatively lower ($917\text{--}930\text{ kg/m}^3$) than HDPE. It is very important plastic material used in industries and household activities. It has a wide area of applications in thermal, electrical and mechanical sectors due to outstanding properties and can be improved by the addition with proper fillers [2]. It is very much chemical resistive and not reactive at room temperature. Its melting point is near about 400 K . It has more branching and weak intermolecular attraction. The branching of LDPE is shown in Fig. 2.1.

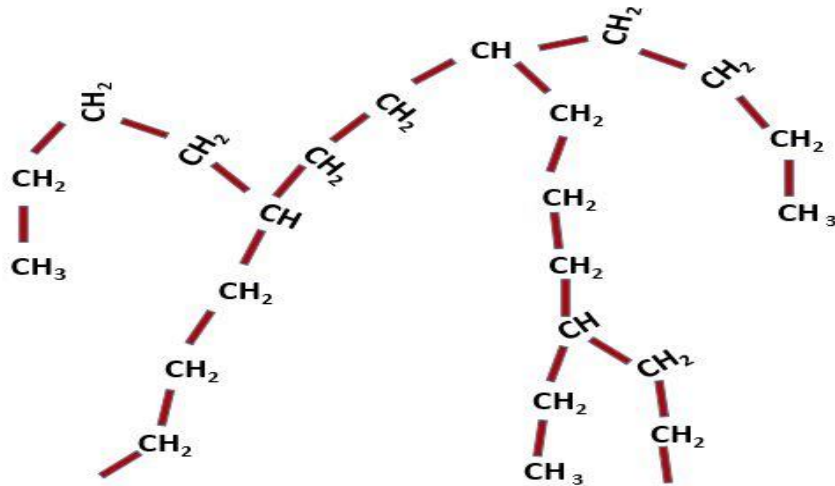


Figure 2.1: Block diagram of branching of LDPE.

The LDPE has a large number of applications [12] in manufacturing various containers, dispensing bottles, wash bottles, wrapping bags, computer components, vehicle and various laboratory equipment. In spite of having a large number of properties and applications LDPE has some limitations in different engineering works owing to low

electrical, thermal and mechanical properties. To overcome these limitations, filler components have to be used. Graphene, the derivative of carbon is redundantly used as filler components in different polymer matrix to enhance the properties [13].

2.3 Graphene

Graphene, a derivative of carbon is synthesized from graphite powder. The graphene is two dimensional [14] carbon compound having single atomic layer of sp^2 hybridization [15]. It is the wonder material which has zero band gap [16]. The graphene has many superficial properties like as, it is the strongest material [17] and conduct heat and electricity [18, 19]. The wonder material graphene is finally discovered in 2004 by two eminent scientist Andre Geim and Konstantin Novoselov at the University of Manchester, hence they were awarded Noble prize in 2010 [20]. The graphene is a single layer hexagonal carbon of interatomic distance 0.142 nm [21]. The newly invented material graphene has a large number of incredible properties. The zero band gap semiconductor graphene has remarkable electron mobility in temperature between 10 K and 100 K [22–24], thermal conductivity is $5300 \text{ Wm}^{-1}\text{K}^{-1}$ [25] and melting point is 4125 K [26]. The graphene has highly strong mechanical properties having the tensile strength 130 GPa and Young modulus is 1000 GPa [18]. The graphene-based products has a large number of application in smartphones, wearable electronics, super power batteries, virtual reality, sports equipment, super-capacitors, flexible capacitor, lightweight vehicles, LEDs, sensor, detector, electronic devices, textile industries etc. [27–32]. Graphene is synthesized from pristine graphite powder in several ways like as [33],

- Chemical vapor deposition (CVD)
- Mechanical exfoliation
- Epitaxial growth
- Organic synthesis
- Chemical method

2.4 Nanocomposite Synthesis Techniques

The polymer matrix nanocomposites can be prepared by different methods, the notable polymer nanocomposite methods are [34]

- In situ polymerization
- Sol–gel method
- Solution casting
- Dip–drying method
- Molding method

2.4.1 Molding method

In the era of modern science and technology material processing, molding and shaping are very important due to abundant applications in our daily life. The frequently used household vessel and industrial instruments such as bottles, cases, electronic accessories, etc. are the most common application of molding techniques. Molding is a technique of manufacturing through which plastic, metal, rubber, powder etc. material are molded and mixed. There are many techniques for molding materials in the world. Among all them the notable methods are,

- i. Compression Molding
- ii. Blow Molding
- iii. Injection Molding
- iv. Extrusion Molding

2.4.1.1 Extrusion molding

Extrusion is one of the most popular technique for fabricating materials in laboratory and industry. It is also a process of manufacturing long products of persistent cross-section in which materials in form of pellets are fed into the machine for molding and mixing. Extrusion of polymers is continuous process and is totally depends on the raw pellets are supplied. The extrusion molding technique is used in the manufacturing industry mainly for process thermoplastics, elastomers and thermosets. The machine used for this technique is known as extrusion molding machine (EMM).

2.5 Extrusion Molding Machine (EMM)

The EMM is a machine in which materials are allowed to feed through the machine and after melting and mixing by using screw and heater the liquid mixtures are ejected through the nozzle of the machine. It is extensively used in manufacturing industry to make pipes, hoses, rods, household equipment, etc. In this process the granules are melt into a liquid and forced through a die to shape. The shape of the die determines the shape of the product. One of the most famous products of extrusion molding is the optical fiber cable. However this machine is fabricated by a large number of equipment's. The first thermoplastic extrusion machine was designed in 1935 by Paul Troester and his wife Ashley Gershoff in Hamburg, Germany and a few later, Roberto Colombo of LMP developed the first twin screw extruders in Italy [35]. Basically two types of extruders are available such as, continuous and reciprocating extruder. The continuous extruder delivers a constant flow of resin as the screw turns, while the reciprocating screw moves not only in a circular motion, but also horizontally within the barrel. As the screw turns, it fills the barrel with materials, thus pushing the screw backwards. When the backward motion of the screw reaches a fixed distance, a hydraulic cylinder is actuated pushing the screw forward. This forward motion delivers a flow material and the process is started over once again. A block diagram of EMM is shown in the Fig. 2.2.

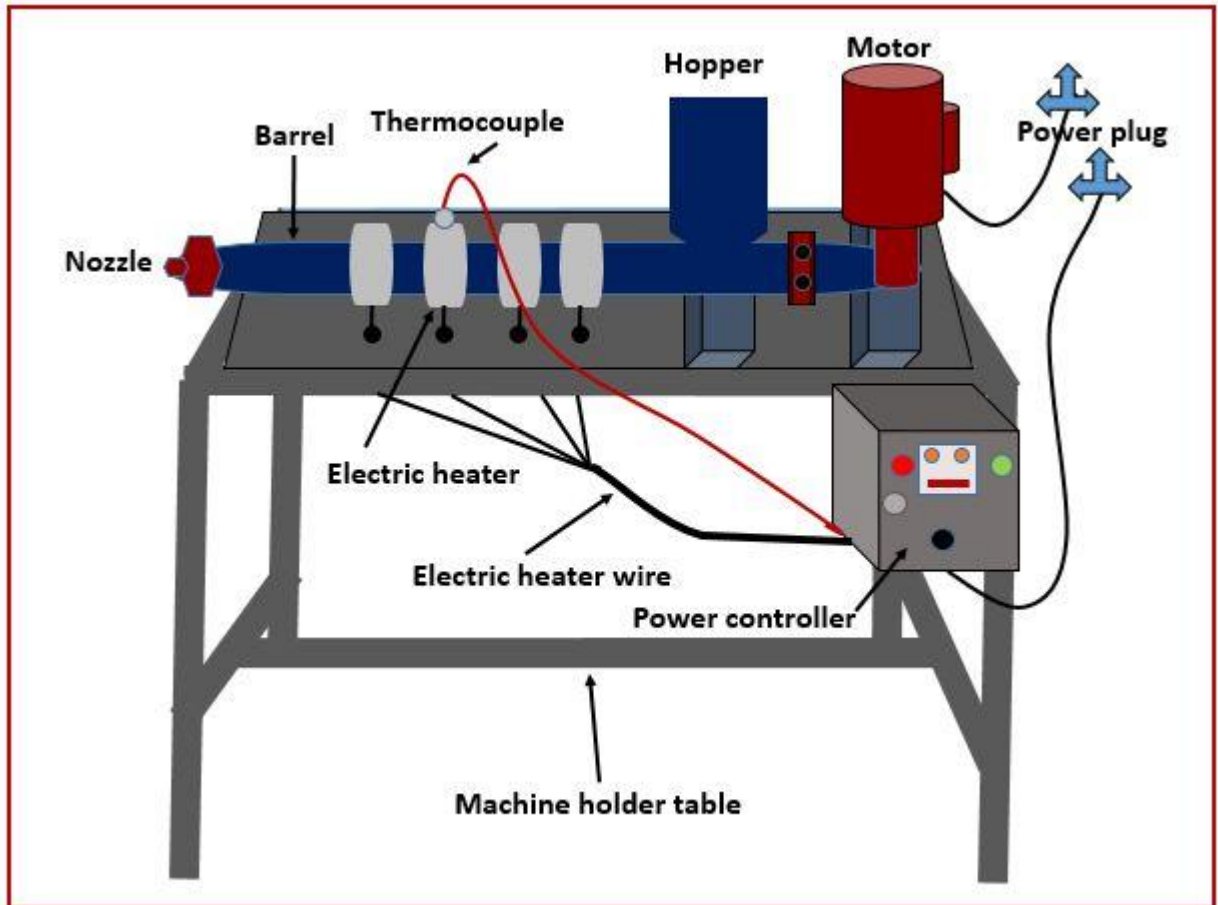


Figure 2.2: A block diagram of Extrusion Molding Machine (EMM).

An EMM is a combination of different components, such as:

- Hopper
- Motor
- Heater
- Barrel
- Nozzle
- Screw

Hopper: The hopper is a large funnel type component which is the main passage of the machine and materials are allowed to send to the barrel for molding and mixing.

Motor: A motor is an electric machine that converts electrical energy into mechanical energy. A motor is attached with the extrusion molding machine to rotate the screw of the machine. The rotation of the motor is controlled according to machine's requirement.

Heater: An electric heater is essential for any types of moldings machine to provide sufficient thermal energy to the barrel. Generally electric ring heater is used so that the barrel can be surrounded by the heater and can supply heat to whole body of the barrel.

Barrel: The barrel is a long hollow horizontal cylinder which holds materials during melting and mixing. It is heated by the use of some heating jackets which are controlled by a power controller.

Nozzle: A nozzle is a part or device which is designed to eject the molded material. It is a pipe or tube that is used to control the velocity and rate of flow of the ejecting fluid.

Screw: The most important part of the extruder is screw. The screw is the heart of the extruder and a key component of any extrusion system which is rounded by the barrel. A motor is adjusted to rotate the screw. It is used to crush and mix the material.

2.5.1 The screw design

Most extruders are equipped with screw as their main mixing component. The extruders are classified as single, double or multiple screw extruders. The single screw extruder has only one screw and the double screw extruder has two screw though both are same in functional operation [36]. Single screw extruders are the most common type of extruders used in the polymer industry, because of its easy design, low costing, and reliability. A block diagram of extruder screw is shown in Fig. 2.3.

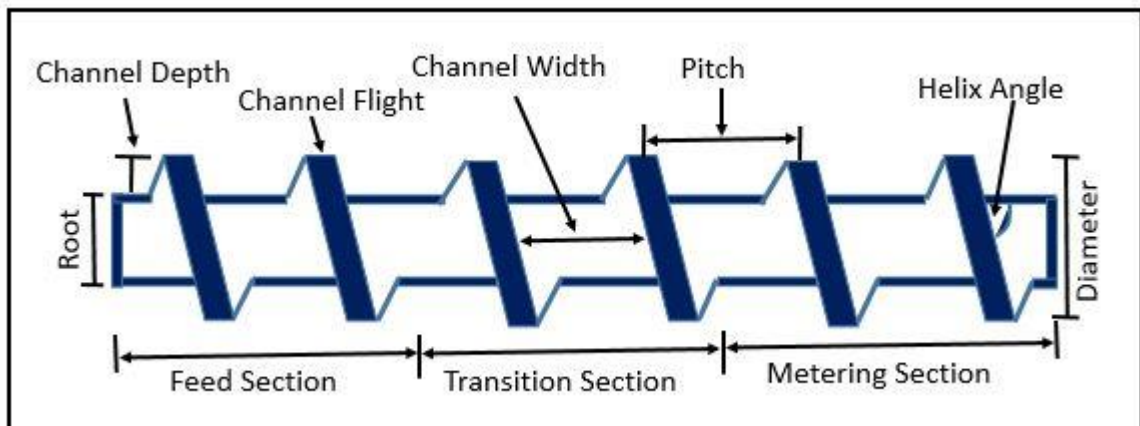


Figure 2.3: A block diagram of single screw extruder design.

Generally the screw of EMM is divided into three division according to its operation, such as,

- Feed Section
- Transition Section
- Metering Section

Feed Section: The feed section is the part of the screw where the unmolded polymer enters into the barrel. The rotating screw moves the material along the heated barrel where it starts to melt.

Transition Section: Materials enter this section at the point where the channel depth of screw starts to decrease. The primary function of the transition section is to compress and melt the material. Materials must be molded before leaving the transition section.

Metering Section: Finally, the material enters the metering section. In this section, pressure is generated which enables the material to be forced into the shaping area. In this section, the channel depth of this screw section is constant.

2.5.2 The screw variables

The screw is the key parts of an extruder that has some worth facts called screw variable.

The worth discussing screw variables (Fig. 2.3) are given below:

- L/D ratio
- Channel depth
- Pitch
- Helix Angle
- Compression ratio
- Channel width

L/D Ratio: The L/D ratio of the screw is the ratio of the flighted length (L) to its outside diameter (D). The ratio is calculated by dividing the flighted length of the screw by its diameter. The greater opportunity of mixing is dependent on the L/D ratio. The higher the ratio will increase the molding and mixing rate.

Channel Depth: The distance between channel root and channel flight is the channel depth. The channel depth influence the degree of shear heat developed by the screw.

Pitch: The pitch of the screw is defined as the distance between two consecutive channel flights. The screw flight pitch is directly related to the helix angle. If the pitch is designed to equal to the screw diameter, it is called the square pitch.

Helix Angle: Helix angle is the angle between the screw flight and the plane perpendicular to the screw axis. It is denoted by ϕ . A relation between helix angle and pitch is given below:

$$\tan\phi = \frac{\text{Pitch}}{\pi D} \dots \dots \dots (2.2)$$

Where D is the screw diameter.

Compression Ratio: It is an important parameter to assess during screw design. Compression ratio can be defined by the ratio of the channel depth in the feed section to that in the metering section. The higher the compression ratio, the greater the shear heat imparted to the sample.

Channel Width: The distance between two consecutive channels is known as channel width. The duration of the residence of materials inside the barrel depends on the channel width.

2.5.3 Operation of EMM

The operation of EMM is a combination of several functions that work simultaneously during operation of the machine [37]. In this process, plastic material in the form of pellets is poured into the hopper and then these are allowed to enter to the barrel. The rotating screw pushes the material forward into the barrel. The barrel heater is set up using an electric heater as per the melting point of the plastic. In the feed zone, the plastic pellets melt gradually as they are pushed through the barrel. The plastic material is completely melted in the melting zone. A thermocouple is used to count the temperature of the barrel. The materials can be overheated by frictional force, thus it should be minimized by using cooling fan or water cooling system. The back pressure gives uniform melting and proper mixing of the molten plastic material into the barrel. A nozzle is used to eject the liquid mixture. After passing through the nozzle, molten plastic enters into a die or they are collected by a tray. The die gives the desired shape of plastic product. These molten plastics are then dried for several hours. The extruded product of an EMM is dependent on melting point of plastic, speed of screw and extrusion pressure.

2.5.4 Advantages/ disadvantages of EMM

The EMM has a large number of advantage such as, low cost, flexibility of operation, continuous and auto-operation, high production rate, multiple times of molding and mixing of material, good mixing, etc. In spite of these advantages it has some disadvantages like as, variation in size of product, lack of perfect ratio of wt% of filler and matrix, high initial cost setup, working risk in high temperature, risks of proper dispersion, need extra manpower, etc.

2.6 Surface Morphology

The surface Morphology is a qualitative and quantitative evaluation of the three dimensional shape of a surface. It is the best evaluation using imaging technique which can also provide layer thickness and other quantitative information. Also it is very important for the research of material science especially for nanomaterial. Surface morphology has special consequence since the properties of nanomaterial are strongly correlated to shape.

2.6.1 Field emission scanning electron microscopy (FESEM)

FESEM has attracted redundant attentions to material scientists for its fruitful applications in science and technology. It is a type of electron microscope that produces images of a sample by scanning the surface with focused ion beam (FIB) electron. The FESEM can achieve resolution better than 1 nm. The electron interact with the atoms of the samples and produce various signals that contain different information about the samples [38]. The schematic diagram of a FESEM machine is shown in Fig. 2.4.

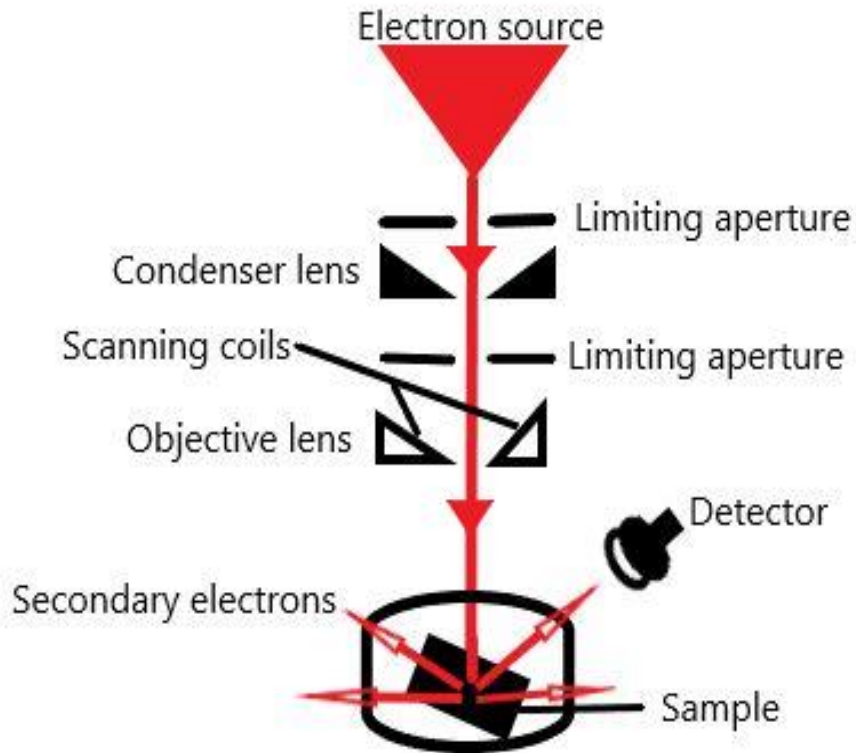


Figure 2.4: Schematic diagram of a FESEM machine.

The electrons ejected from the source interact with the atoms of the sample and different types of signals are formed including secondary electrons (SE), back-scattered electrons (BSE), characteristic X-rays and light, absorbed and transmitted electrons. Among them, the SE are emitted very close to the sample surface. Moreover, SE is very standard equipment and produces very high resolution images.

2.6.2 Transmission electron microscopy (TEM)

Transmission electron microscope (TEM) is an analytical technique in which a beam of electrons coming from a source is transmitted through a sample and yields an image [39]. TEM is a major characterization device in physical and chemical measurements of material science and technology. It has a large number of applications in material science, nanotechnology, biomedical physics, etc. owing to its overabundant advantages. TEM can form images better than any other microscope. The schematic diagram of a TEM machine is shown in Fig. 2.5.

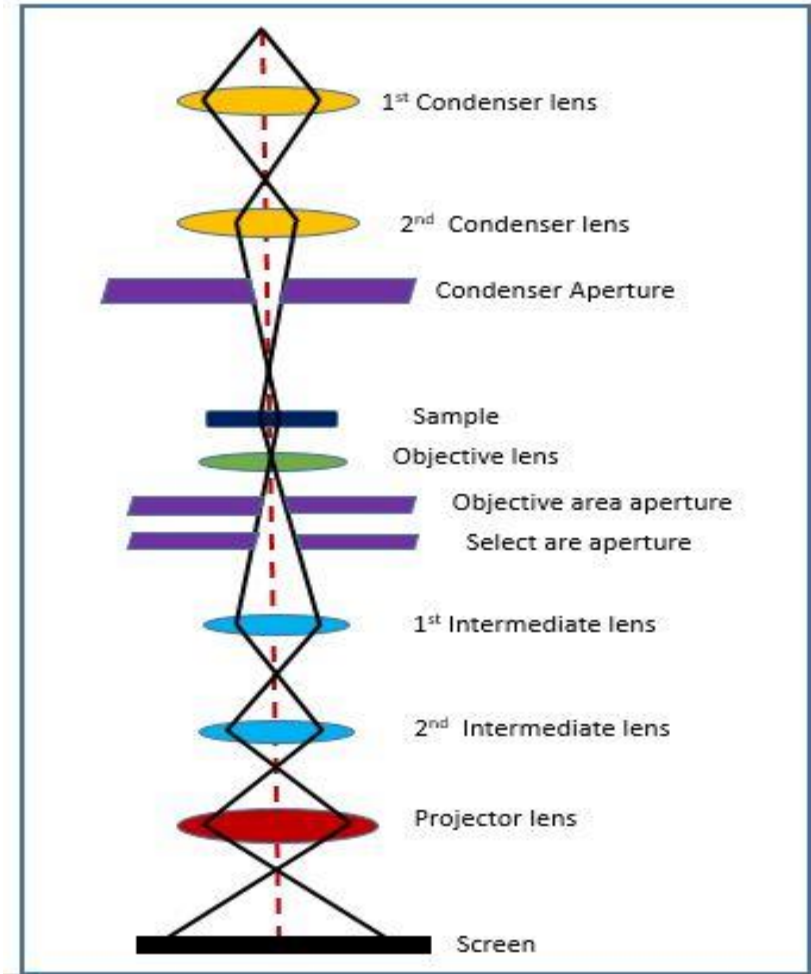


Figure 2.5: Schematic diagram of a TEM machine.

The TEM consists of a large number of equipment's such as, electron emission system, vacuum chamber, electrostatic plates, lenses, phosphor screen, apertures etc. While working the beam of electron is emitted from the electron gun and the emitted beam of electron interacts with specimen and a part of it is transmitted through the sample and images are formed and then the images are magnified and focused onto a fluorescent screen.

2.7 Elemental Analysis

2.7.1 Energy dispersive X-ray (EDX) spectroscopy

Energy dispersive X-ray (EDX) spectroscopy is an analytical technique which is used to measure elemental analysis and chemical composition of a sample material [40]. It is a fundamental material characterization technique which is happened due to the penetration

of electron to the sample. Electrons from source interacts with the atom of sample which knocks out one electron and produce X-rays. In this study, two types of X-rays are produced such as, continuum X-ray and characteristics X-ray. The X-ray produced from the energy difference between two cells is called characteristics X-ray and the X-ray when the beam electron interact with the nucleus of the sample is known as continuum X-ray. The schematic diagram of X-ray production is shown in Fig. 2.6.

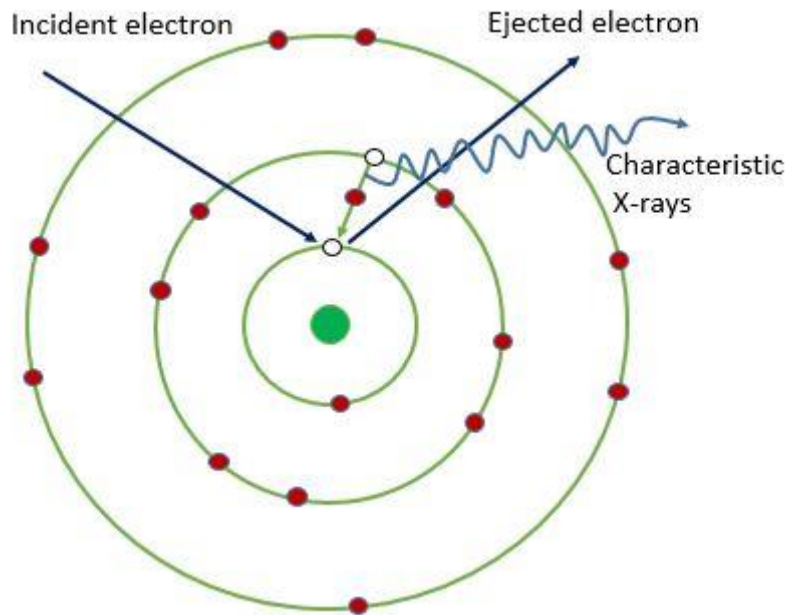


Figure 2.6: Schematic diagram of X-rays production.

High energy electron emitted from a source heats a sample. The incident beam of electron excite an electron in inner shell and eject the electron from its position and create a hole. Then an electron from higher energy shell fills the hole. The difference between the higher energy shell and lower energy shell released in the form of an unknown ray which is then named as characteristic X-ray. These are measured by an energy dispersive X-ray spectrometer (EDS). The main components of an EDS are electron beam, X-ray detector, pulse processor and analyzer. The incident electron is emitted from electron beam and after interaction the ejected electron is recorded by X-ray detector. The recorded information is then sent to pulse processor which measures the signals and passes them into a data analysis analyzer. The principal job of an EDX machine is to observe the presentence of elements present in the composition.

2.8 Structural Analyses

2.8.1 X-ray diffraction (XRD)

When a beam of electromagnetic radiation encounters an obstacle it gets slight bending around the edge of the object, this phenomena is known as diffraction. X-Ray diffraction (XRD) is a technique in which a material is treated as its atomic and molecular structure which shows whether the material is crystal or non-crystal [41]. In crystal, the atoms and molecules are arrange in a periodic pattern and in non-crystal, the atoms and molecules arranged in random orientation. It is a powerful technique for characterizing crystalline materials. It delivers information on crystal structures, phases, crystal orientations, grain size, and crystal defects. Using monochromatic beam of X-rays, peaks are produced by constructive interference of the beam. When the incident rays interact with the samples and produce constructive interference then according to Bragg's law:

$$2d\sin\theta = n\lambda \dots \dots \dots (2.3)$$

Where, n and λ are the integer and wavelength of X-rays, d and θ are the interplanar spacing and diffraction angle respectively. According to this law the interplanar spacing is decreased with the increased of diffraction angle. The relation between the diffraction angle and wavelength of electromagnetic radiation is shown in the Fig. 2.7.

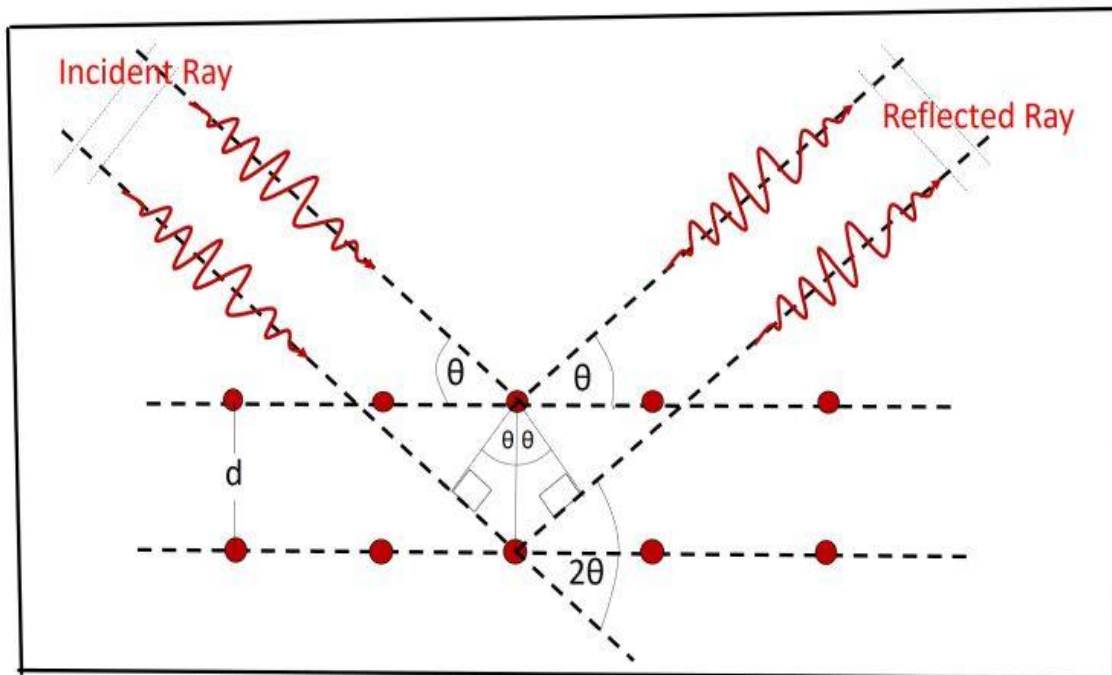


Figure 2.7: Schematic diagram of Bragg's XRD pattern.

The relation between electromagnetic radiation, diffraction angle and lattice spacing of the sample can be seen from this law. The X-ray diffractometer generally consists of three components such as, X-ray tube, sample holder and X-ray detector. The X-rays are produced in a cathode ray tube by heating filament. Then after filtering monochromatic X-rays are allowed to strike the specimen placed on the rotating sample holder. Then the intensity of the reflected X-rays are recorded by a rotating detector. An X-ray diffractometer does the mechanism that the sample rotates in the path at an angle θ and the detector is mounted in such a way that it rotates at an angle of 2θ . A goniometer is used to maintain the angle.

2.8.2 Fourier-transform infrared (FTIR) spectroscopy

FTIR spectrometer is an advanced analytical technique which is used to measure the organic and inorganic materials by measuring absorption of mid-range infrared radiation [42]. The recorded data are allowed to transferred a computer and the computer yields analytical result by using the mathematical method Fourier transform, thus it is called Fourier- transform infrared (FTIR) spectrometer. In this technique, Michelson interferometer is used to perform the experimental work. A schematic diagram of FTIR is shown in Fig. 2.8.

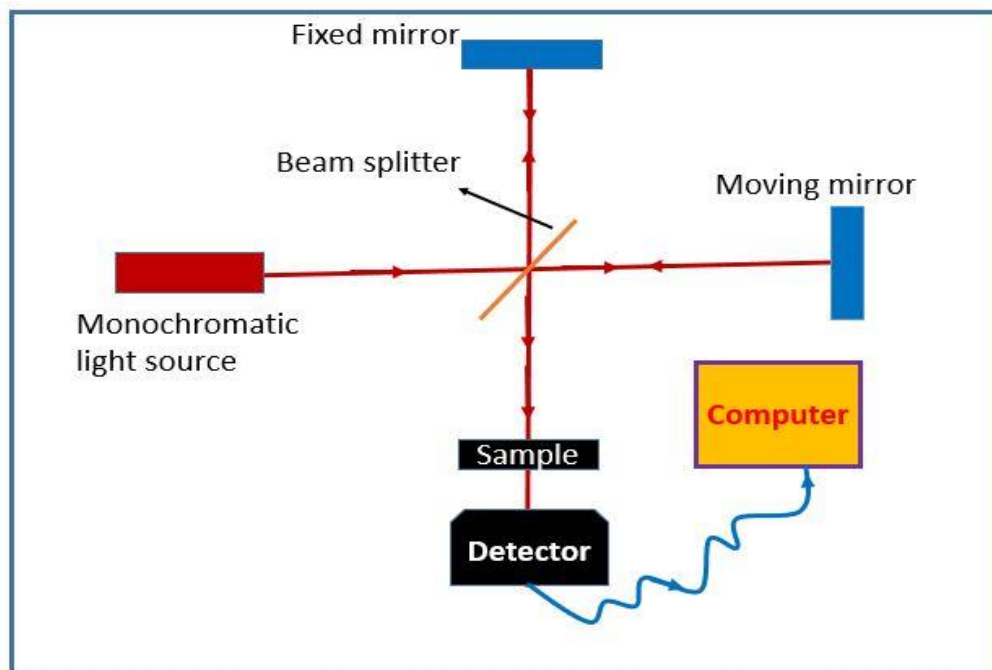


Figure 2.8: Schematic diagram of FTIR.

The instrumental system used in the FTIR experiment is called interferometer. The interferometer generally consists of the equipment's: Monochromatic light source, beam splitter, two mirror, sample, detector and a computer. The emitted monochromatic light splits in two parts in the beam splitter where one part is transmitted to the moving mirror and another part is reflected to the fixed mirror. The two rays after reflection from the two mirror incidents in the beam splitter. The two incident rays afterwards combine together and produce constructive and destructive interference pattern which are called interferogram. The interferogram from beam splitter then heats the sample where some rays are absorbed and some are transmitted. The transmitted rays are recorded in the detector at every wavelength and these are sent to the computer for Fourier transform. FTIR has a large number of applications rather than dispersive spectrometer where in dispersive spectrometer, grating is used. Basically FTIR is largely used to observe the chemical composition of organic compounds for the use of material science, biomedical engineering, nanotechnology, etc.

2.9 Thermal Analyses

Thermal analysis is a branch of science in which properties of materials are monitored with the variation of temperature or time. Several properties of material such as chemical, physical, etc. are revealed with respect to the temperature and time in this method at specified atmosphere. It is necessary to characterize materials and their behavior over a range of temperatures to determine what materials are more stable than others and can withstand without changing. The notable thermal analysis are explained here.

2.9.1 Thermogravimetry/derivative thermogravimetry (TG/DTG) analysis

TG analysis is an analytical technique in which the mass of a material is observed as a function of temperature or time under a controlled atmosphere [43]. Metals, polymers, glass and plastics can be analyzed by the TG analyzer. A schematic diagram of TG analyzer is shown in the Fig. 2.9.

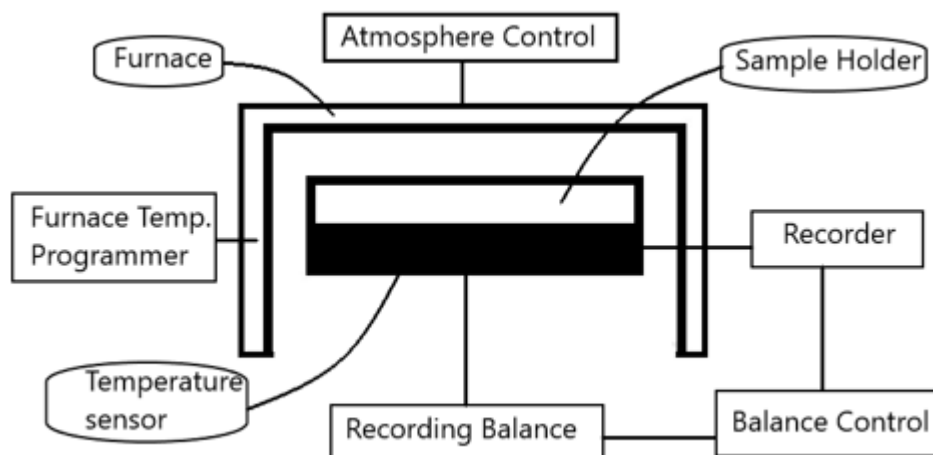


Figure 2.9: Schematic diagram of TG/DTG analyzer.

A TGA machine consists of a sample pan that resides in a furnace and is heated or cooled during the experiment. The mass of the sample is monitored during the experiment. The sample environment is controlled by refine gas that may be inert or reactive gas that flows over the sample and exits through an exhaust. Generally nitrogen, oxygen and air is used in this experiment. The basic principle of TGA is that when a sample is heated, its mass changes and this change is used to determine the composition of a material or its thermal stability. Usually, a sample loses weight as it is heated up due to decomposition. A sample could also gain weight due to oxidation or absorption. Temperature is monitored via a thermocouple. The weight of the sample is plotted against temperature or time to illustrate thermal transitions in the material. The descending TGA thermal curve is displayed from left to right which indicates a weight loss. DTG is defined as the first derivative of TG with respect to temperature. DTG reveals the decomposition of the constituents of organic matter at specific temperature with the help of peaks during DTG analysis. In DTG, it is the rate at which the loss/gain of weight occurs in a thermo-balance. In most of cases a reliable qualitative and quantitative evaluation of the TG curve is impossible without having its first derivative (DTG). The DTG peak height at any temperature gives the rate of mass loss. With DTG curve the actual peak can be precisely determined in overlapping reactions.

2.10 Mechanical Strength

Mechanical engineers are highly concern about the mechanical properties of material due to the importance of material in the era of science and technology because materials are largely responsible to improve the technology. The materials are treated as how they can be deform or break as a function of applied force, time and temperature. The results of the tests also dependent on the size and shape of the specimen. The fundamental parameter of mechanical strength test are stress, strain, elongation, compression and sheer. There are different type’s parameter to test material such as,

- Hardness
- Tensile strength
- Impact testing
- Fracture toughness testing
- Creep testing
- Fatigue testing

2.10.1 Tensile Strength

Tensile strength is a properties of material which can be defined as the ability of material that withstand load without fracture. It measures the force that pull something to the point where it breaks. The maximum amount of force that it can be subjected to before fracture of the specimen is known as ultimate tensile strength (UTS). It is very important and it has a large number of applications in material science and infrastructure engineering [44]. The ultimate tensile strength (UTS) formula is:

$$UTS = \frac{\text{Ultimate force (F)}}{\text{Cross-sectional are (A)}} \dots \dots \dots (2.4)$$

And the Young Modulus is:

$$\text{Young Modulus, } Y = \frac{\text{Tensile Stress}}{\text{Tensile strain}}$$

$$\Rightarrow Y = \frac{F/A}{l/L} \dots \dots \dots (2.5)$$

Where l and L is the changed length and initial length respectively.

The UTS and Young Modulus can be calculate from the equation (2.4–2.5).

A block diagram of tensile strength measurement is shown in Fig. 2.10.

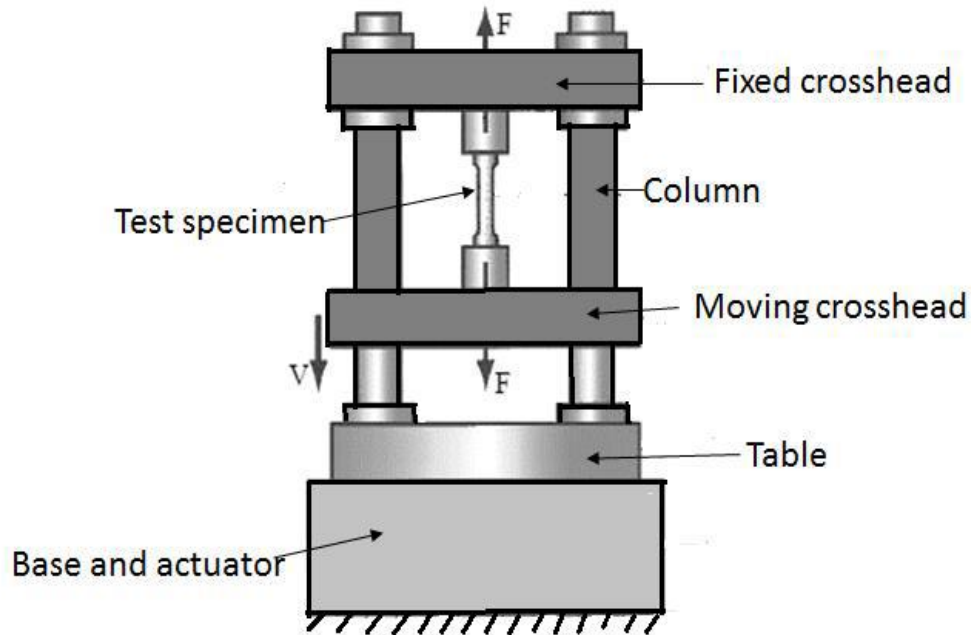


Figure 2.10: Tensile strength measurement setup.

When equal and opposite forces are applied simultaneously at both the ends that pulls the material, it tries to elongate and the diameter reduces. Due to the stretching of the specimen, the initial test specimen length is increased and area is reduced. The general idea of operation of tensile test is to place a sample between two grips which clamp the sample. Then load is applied to the material gripped at one end while the other end is fixed. The load is increased until the specimen is fractured. From the measurement of tensile it can be known that the material is ductile or brittle.

2.11 Electrical Properties

Electrical Properties of any material expresses its inherent and fundamental properties. Mainly it reveals the mobility of charge carrier [45]. The mobility of charge carrier depends on the classification of material such as, conductor, semiconductor and insulator. These classes are explained by band gap. The band gap of conductor is zero, the semiconductor has a moderate type of band gap which is near about 1 eV and the insulator has a large number of band gap, i.e. there are a large number of distance between the two bands which

is near about 15 eV. Polymers are in general an insulating materials. The band gap between valance and conduction band in polymer is near about 15 eV. They can be semiconductor by introducing an additive of filler agent. The additive materials are normally highly conductive materials. After the addition of filler agent the final composite material is revealed its properties as semiconductor or conductor.

2.11.1 Conductivity measurement setup

There are two possible methods to measure dc electrical conductivity such as, two probe methods and four probe methods. In the two probe measurement, the sample is simultaneously contacted in two positions, whereas in the four probe measurement, the sample is simultaneously contacted at four positions to measure its conductivity. While the difference in these two methods may seem minor at first glance, there is a specific issue with the two probe measurement which is effectively addressed by the four probe measurement. Though four probe method is used to eliminate the contact resistance between sample and probe, the two probe method is largely used to engineers and scientist for its relaxed circuit connections and operations [46]. A block diagram of two probe method is shown in Fig. 2.11.

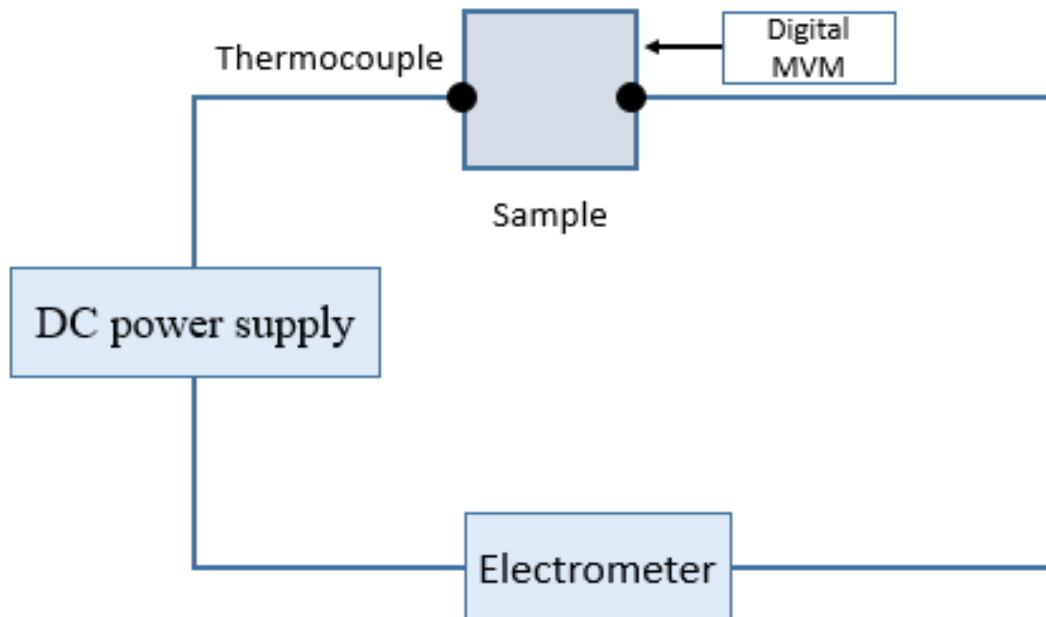


Figure 2.11: Two probe method circuit diagram.

2.11.2 DC current density

Current density is defined as the electric current per unit area of cross section. It is a vector quantity which is defined by J . If we consider a small piece of specimen whose area of cross section is 'A' and the flowing current is 'I' then the current density can be defined as:

$$J = \frac{I}{A} \dots \dots \dots (2.6)$$

The current density is very important in laboratory and industry for manufacturing all types of electrical equipment since all the circuit performance totally depend on specific current density.

2.11.3 DC electrical conductivity

The electrical conductivity can be defined as the measure of a materials ability to allow the transport of an electric charge. Electrical conductance is an electrical phenomenon where a material contains movable particles with electric charge, which can carry electricity. When a potential difference is placed across a conductor, its electrons flows, and an electric current appears. The electrical conductivity depends on the classification of materials such as: conductor like material has high conductivity, insulator like material has low conductivity and a semiconductor like material has a conductivity in between conductor and insulator. Considering a piece of sample of length L, resistance R, area of cross section A, then the electrical conductivity can be written as:

$$\sigma = \frac{L}{RA} \dots \dots \dots (2.7)$$

Electrical conductivity is a property of materials that determines how well a given material conduct electricity. Electrical conductivity is a property of the material itself, while electrical conductance is a property of a particular electrical component [47]. Electrical conductivity can be defined as how much voltage is required to get an amount of electric current to flow. Materials with high conductivity, like copper and aluminum, are called conductors. Generally, most metals have high conductivity, because the electrons in their outermost shell can move easily.

2.11.4 Activation energy

The minimum amount of energy required to get started a reaction is known as activation energy. It is denoted by E_a or ΔE . Chemical reactions also need energy to be activated. They require a certain amount of energy just to get started. A chemical reaction happens only if the particles are move and they take energy to break the threshold stage. The activation energy is closely related to temperature, reaction rate and kinetic energy of the particles associated with the reaction [48]. These parameters are relates in an equation designed by a Swedish scientist named Svante Arrhenius, in 1889. Thus the equation is known as Arrhenius equation, which can be written as:

$$k = A \exp\left(-\frac{E_a}{RT}\right) \dots \dots \dots (2.8)$$

Where, k is the reaction rate, A is frequency factor, E_a is activation energy, R is universal gas constant, and T is the absolute temperature. For more convenience, this equation (2.8) can be written as:

$$\ln k = \ln A - \frac{E_a}{RT} \dots \dots \dots (2.9)$$

By calculating slope from the equation (2.9), the activation energy can be calculated.

2.11.5 Dielectric properties

The study of frequency dependent electrical properties are very essential in science and technology. A material that can store energy when a voltage is applied causing electric polarization is known as dielectric property. The dielectric material is an insulator or a very poor conductor of electric current. When dielectrics are placed in an electric field, practically no current flows in them because of their zero electron mobility. When electric polarization occurs in the dielectric, the positive and the negative charges are displaced in the direction opposite to the electric field. The capacitance of a capacitor filled with dielectric material is greater than in vacuum. The dielectric constant is the ratio of the permittivity of a substance to the permittivity of free space. It is equal to the ratio of the capacitance of a capacitor filled with the given material to the capacitance of the same capacitor in vacuum without the dielectric material [49]. It is denoted by ϵ_r ,

$$\epsilon_r = \frac{C}{C_0} \dots \dots \dots (2.10)$$

Where C is the value of the capacitance of a capacitor filled with a given dielectric and C₀ is the capacitance in vacuum is measured as,

$$C_0 = \frac{\epsilon_0 A}{d} \dots \dots \dots (2.11)$$

Where ϵ_0 is the permittivity in vacuum, ‘A’ and ‘d’ are the area and thickness of the dielectric, respectively.

The permittivity (ϵ) has the real and imaginary part such as,

$$\epsilon = \epsilon_r - j\epsilon_{rr} \dots \dots \dots (2.12)$$

Where, ϵ_r and ϵ_{rr} are the dielectric constant (relative permittivity) and dielectric loss factor. The ratio of the dielectric loss to the dielectric constant is known as loss tangent [50], which is calculated as,

$$\tan\delta = \frac{\epsilon_{rr}}{\epsilon_r} \dots \dots \dots (2.12)$$

By calculating these equations the dielectric properties can be measured.

CHAPTER 3

EXPERIMENTAL DETAILS

3.1 Materials

The materials and instruments used in this thesis are given below:

- Extrusion molding machine (EMM), Homemade.
- Graphite Powder, Particle size 95%, Qualikems Fine Chem. Pvt. Ltd., India.
- Sulphuric Acid (98%), Merck KGaA, 64271 Damstadt, Germany.
- Potassium Permanganate, Merck KGaA, 64271 Damstadt, Germany.
- Sodium Nitrate, Merck KGaA, 64271 Damstadt, Germany.
- Hydrogen Peroxide (30%), Merck KGaA, 64271 Damstadt, Germany.
- Hydrazine Hydrate (80%), Merck KGaA, 64271 Damstadt, Germany.
- Low density polyethylene (LDPE) Pellets, BASF, Germany.

3.2 Apparatus Used For This Work

3.2.1 Analytical balance meter with

An analytical balance is a class of balance that is designed to measure mass of material and chemical in small range. It is also used to measure accurate and precise weight of sample. The balance meter that is used in this experiment is highly sensitive and can measure sample to nearest tenth of a milligram (0.0001g). Fig. 3.1 shows a photo of the Analytical Balance Meter.



Figure 3.1: Analytical Balance Meter (Left) and Hot plate with magnetic stirrer (Right).

3.2.2 Hot plate with magnetic stirrer

Magnetic stirrer is a very important laboratory equipment that is mainly used to mix different chemicals within a beaker. There is a small bar magnet in the stirrer which rotates due to magnetic field and mix the chemicals. There is a heating system in the device to control the desired heat. To synthesis any chemical this is very useful and helpful to get a homogeneous solution. The magnetic stirrer used here is XMTD-701, China. Fig. 3.1 shows an image of the hot plate magnetic stirrer.

3.2.3 Ultrasonic bath

The apparatus Ultrasonic bath uses the application of ultrasound (>20 kHz) to perform the laboratory work. The process of sonication is the act of applying sound energy to agitate particles in a sample. It is used for various purposes such as the extraction of multiple compounds from another compounds or plants. This processes can be carried out by the use of a probe-type ultrasonic homogenizer or an ultrasonic bath. The ultrasonic bath used in this research work is shown in Fig. 3.2.



Figure 3.2: Photograph of Ultrasonic bath (Left) and centrifuge machine (Right).

3.2.4 Centrifuge machine

A centrifuge machine is a laboratory equipment that is used to wash chemical by using rotational force. The machine works using the sedimentation principle, where the centrifugal acceleration causes denser substances or particles move towards the center

and settle to the bottom of the sample tubes and lighter particle rise up. Fig. 3.2 shows an image of the Centrifuge machine.

3.2.5 Universal hot air oven

A hot air oven is very important laboratory apparatus in any sample fabrication to have the heat treatment of the sample. It is an electrical instrument mainly used to dry materials. The temperature range of this oven is around 300–1200 K. A thermostat is used to control the temperature. Its double walled insulation keeps the heat in and conserves energy. The oven used here (Cowbell, India) is shown in Fig. 3.3.



Figure 3.3: A photograph of universal hot air oven.

3.3 Fabrication of extrusion molding machine (EMM)

The EMM, used in this research was fabricated from a local market. The necessary equipment used to fabricate the machine with full specifications are given below:

- (i) Hopper size: Upper part: (5×5) inch²; Lower part: (1.4×3.4) inch².
- (ii) Barrel: Outer Diameter: 2 inch; Inner diameter: 1 inch.
- (iii) Barrel length: 20 inch.
- (iv) Screw diameter: 1 inch.
- (v) Screw length: 25 inch.
- (vi) Motor power: 0.5 HP.
- (vi) Nozzle diameter: 0.2 inch.
- (viii) Maximum temperature: 676 K.

The full specification of EMM is shown in Fig. 3.4.

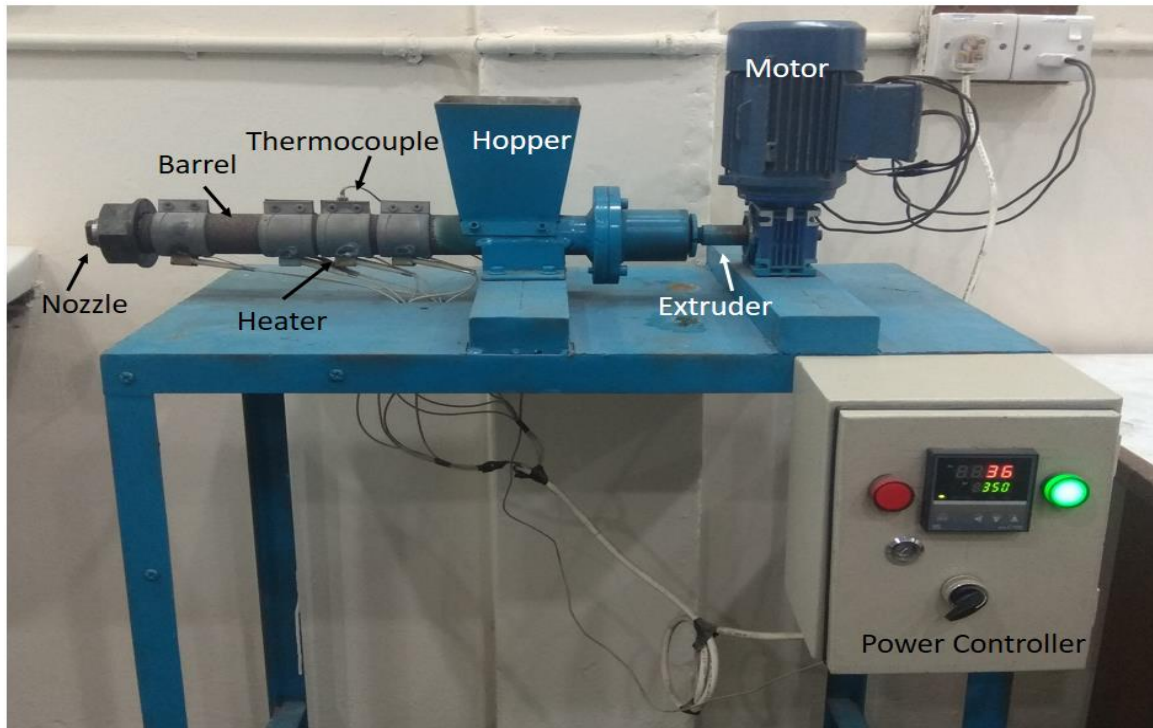


Figure 3.4: Extrusion Molding Machine (EMM) set up.

3.4 Composite Fabrication

3.4.1 RGO synthesis

RGO was prepared by the following method. 2 gm of graphite powder and 2 gm of NaNO_3 was added to 50 ml of H_2SO_4 (98%) with continuous stirring in a hot plate with magnetic stirrer by keeping the temperature below 280 K by an ice bath. The mixture was stirred for 2 hours at the same temp and 6 gm of KMnO_4 was added to the suspension very slowly with continuous stirring. Then the ice bath was removed, and the sample mixture was stirred at 303 K till it become pasty brownish color and kept under stirring for 2 hours. After that the solution was weakened with the slow addition of 100 ml of distilled water. The reaction temperature was increased quickly to 370 K and the color was changed to brown type. Further the solution was weakened by the addition of 200 ml of distilled water under continuous stirring. Finally the solution mixture was treated with 8 ml H_2O_2 to terminate the reaction indicated by the formation of paste into yellow color. For purification, the mixture was washed by centrifugation with ethanol for several times. After filtration the solution was dried in a hot oven at about 370 K for 24 hours. Finally, the graphene oxide (GO) was obtained as flake and grinded to obtain powder form. Afterwards,

to obtain RGO, 2 gm of GO was dispersed with 400 ml of distilled water and the mixture was treated in an ultrasonic bath for 1 hour. Then 20 ml of hydrazine hydrate was added to the solution mixture, keeping stirring for 2 hours at about 370 K. Then the solution was turned into black color and pH of the solution was fixed about 10. The Precipitated mixture was dried for 72 hours at 370 K. Finally RGO was obtained as dark black powder. The RGO synthesis mechanism flowchart is shown in the Fig. 3.5.

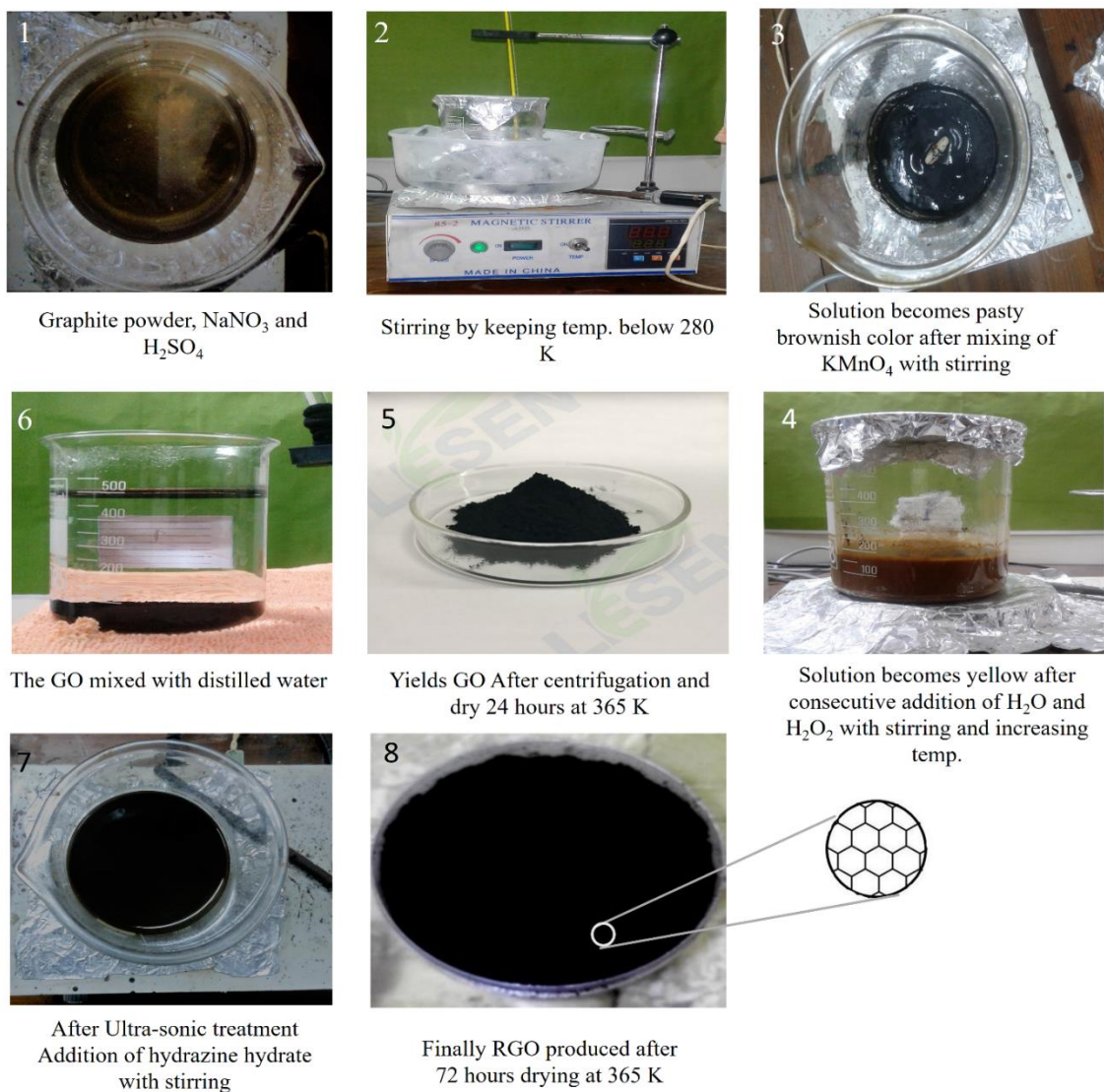


Figure 3.5: Flowchart of GO and RGO synthesis.

3.4.2 RGO/LDPE Nanocomposite

To obtain LDPE/RGO nanocomposite, 100 g of LDPE pellets and 2 g RGO was mixed properly in a small vessel. Then the mixture was poured into the hopper of the extrusion molding machine. Afterwards the machine was switched on and the barrel temperature was adjusted to 430 K. The mixtures were melted by dint of the rotational force of the extruder as well as the heating power of the electric heater. Afterward the molded material was pressurized by the extruder automatically to be ejected through the nozzle and finally, the ejected materials were collected by a tray. Then after keeping 25–30 minutes in room temperature the materials were dried and was revealed as nanocomposite sheet. The sheet was then be cut into required shapes for different characterization. The RGO/LDPE nanocomposite preparation flowchart is shown in Fig. 3.6.

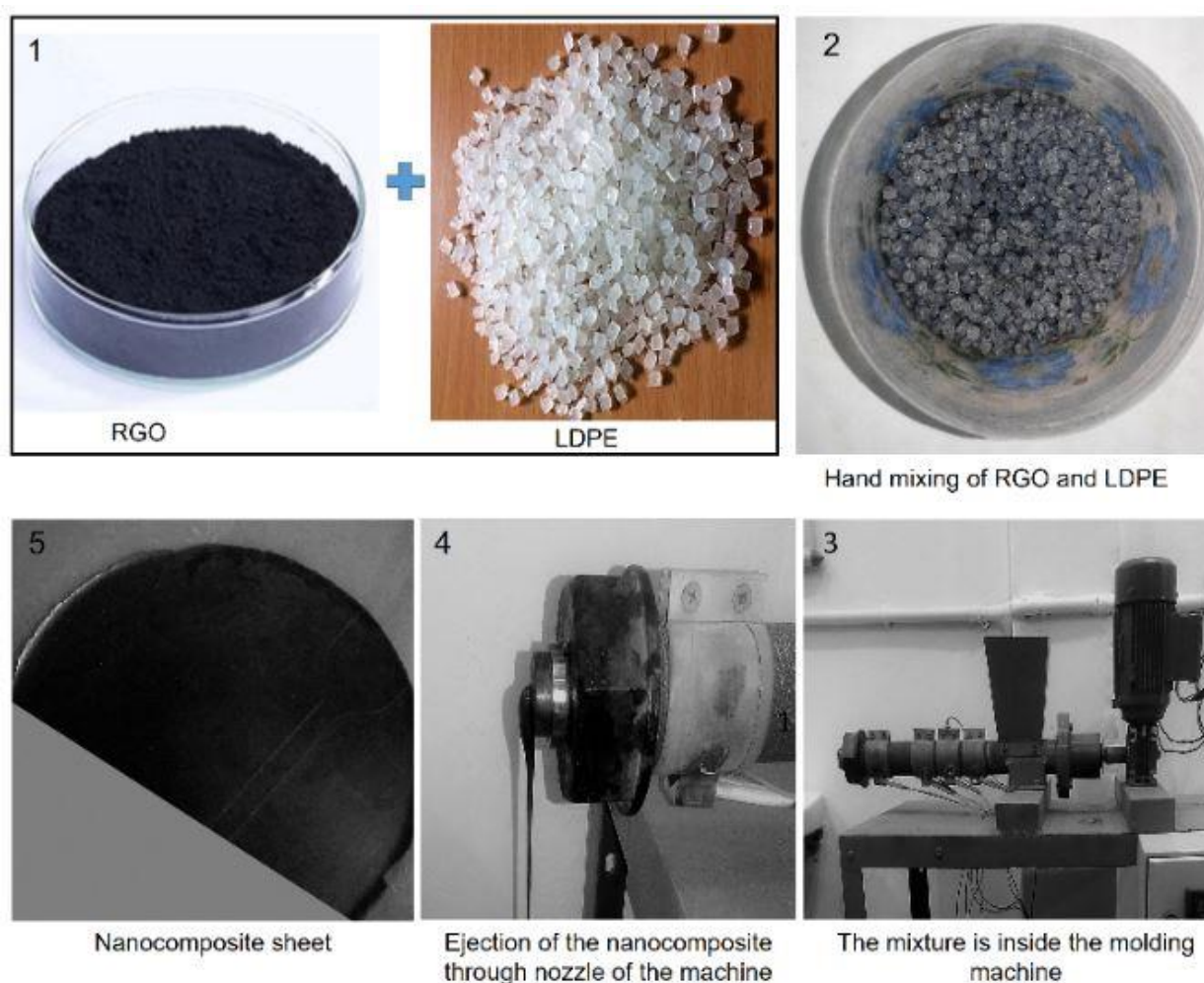


Figure 3.6: RGO/LDPE nanocomposite preparation flowchart.

3.5 Characterization of the Composites

Having synthesized the RGO and RGO loaded RGO/LDPE nanocomposite by EMM process, the samples were cut into desired shape for different characterization.

3.5.1 Surface morphology

The surface morphology of the nanocomposites is observed by using field emission electron microscopy (FESEM, JEOL JSM-7600F). FESEM images are captured at 3k-100k magnifications. The FESEM set up is shown in the Fig. 3.7.



Figure 3.7. Field emission scanning electron microscope (FESEM) set up.

3.5.2 Elemental analysis

Energy Dispersive X-ray Spectroscopy (EDX) is a chemical microanalysis technique used in conjunction with FESEM. The operation parameters for the EDX analysis are as follows: accelerating voltage of 10 kV, probe current of 1 nA, energy range of 0 – 20 keV. The EDX measurement results was taken by the same instrument like as FESEM measurement.

3.5.3 Structural analysis

3.5.3.1 X-ray diffraction

The X-ray diffraction (XRD) measurements of the fabricated composites were recorded by PANalytical Empyrean model X-ray diffractometer (USA). The machine is equipped with curved graphite monochromator high-intensity $\text{CuK}\alpha$ radiation ($\lambda = 0.154 \text{ nm}$) and operated at 45 kV and 40 mA. The diffractograms are recorded in the range of angular region (2θ) from 10° to 90° . Step size 0.0066° , $k_2 1.544426$. The XRD measurement setup is shown in the Fig. 3.8.



Figure 3.8: X-ray diffractometer set up.

3.5.3.2 Fourier transform infrared (FTIR) spectroscopy

The FTIR spectroscopy test is mandatory to investigate the chemical structure of materials. The FTIR spectroscopy (Shimadzu, Japan) is shown in the Fig. 3.9.



Figure 3.9: A photograph of FTIR setup.

3.5.4 Thermal stability

The Thermogravimetric (TG) analysis and derivative thermogravimetric (DTG) is a method of thermal analysis in which changes in physical and chemical properties of materials are measured as a function of increasing temperature or time. The instrument that is used to measure the TG/DTG is SII EXSTAR 6000 TG/DTA 6300, Seiko Instruments Inc., Japan. The thermal analysis by this machine is done in N₂ environment. A photograph of this instrument is shown in the Fig. 3.10.



Figure 3.10: TG/DTG measuring setup.

3.5.5 Mechanical strength

Mechanical strength measurement is very important for material science specially for the application of automobile, aero plane, etc to investigate whether the used materials are suitable or not. The instrument used for this test is universal testing machine (UTM) from Shenzhen Wance Testing Machine Co. Ltd, China. For this characterization the samples are cut into the following size: gauge length = 30 mm, width = 12 mm, thickness = 4 mm. A photograph of this instrument is shown in the Fig. 3.11.



Figure 3.11: A photograph of tensile strength measurement setup.

3.5.6 Electrical measurement

3.5.6.1 DC electrical measurement

For the electrical measurement the sample was cut into the shape of 7.5 mm diameter and 2 mm thickness and the sample was coated with silver paste to make electrode. Afterwards the sample was inserted inside a pressure contact. Then the current was measured at different voltages and temperature. The voltage is supplied by a stabilizer power supply (6545A, Agilent, Japan) and current is measured by a digital Keithley 6517B electrometer (USA). The temperature-dependent electrical measurement of the samples are measured in the temperature range of 303–363 K by heating the samples with an isolated chamber. The DC electrical measurement set up is shown in the Fig. 3.12.



Figure 3.12: DC electrical measurement set up.

3.5.6.2 AC electrical measurement

The ac electrical measurement was carried out by shaping the samples like dc measurement. The instrument used for ac measurement is Wayne Kerr 6500B, UK. A photograph of this machine is shown in Fig. 3.13.



Figure 3.13: AC electrical measurement set up.

CHAPTER 4

RESULTS AND DISCUSSION

4.1 Surface Morphology

The surface morphology of RGO, pure LDPE and RGO loaded RGO/LDPE nanocomposites are discussed.

4.1.1 Surface morphology of RGO and RGO/LDPE nanocomposite

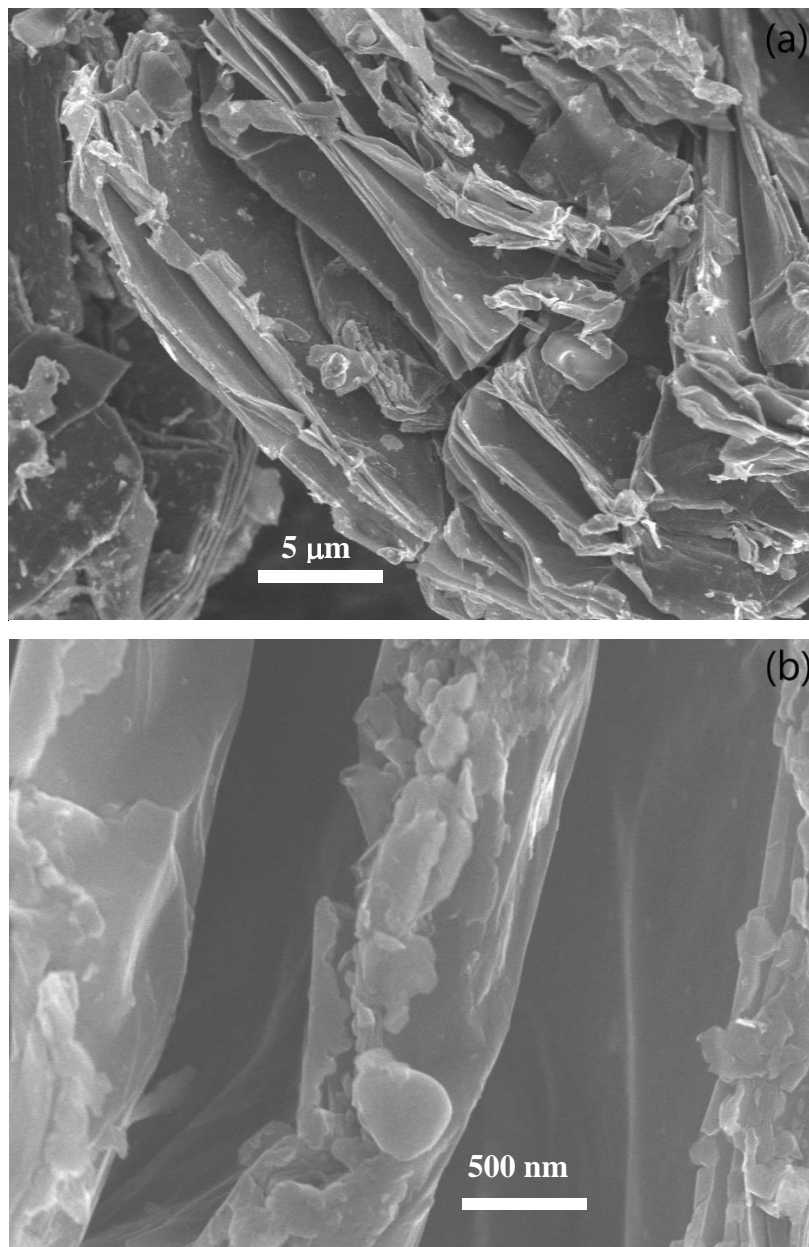


Figure 4.1: FESEM images of RGO at (a) $\times 3k$ and (b) $\times 30k$ magnification.

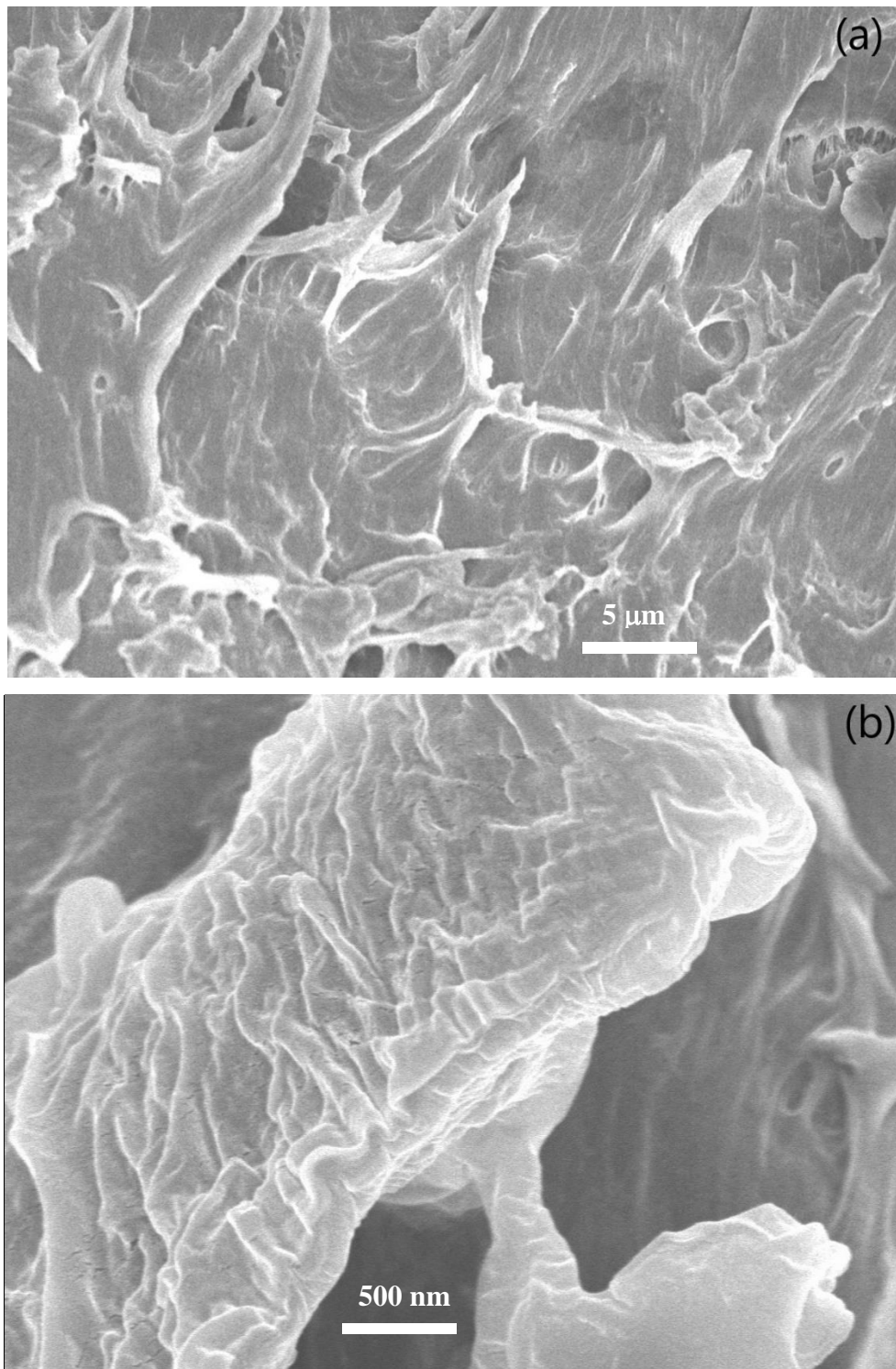


Figure 4.2: FESEM images of pure LDPE at (a) $\times 3k$ and (b) $\times 30k$ magnification.

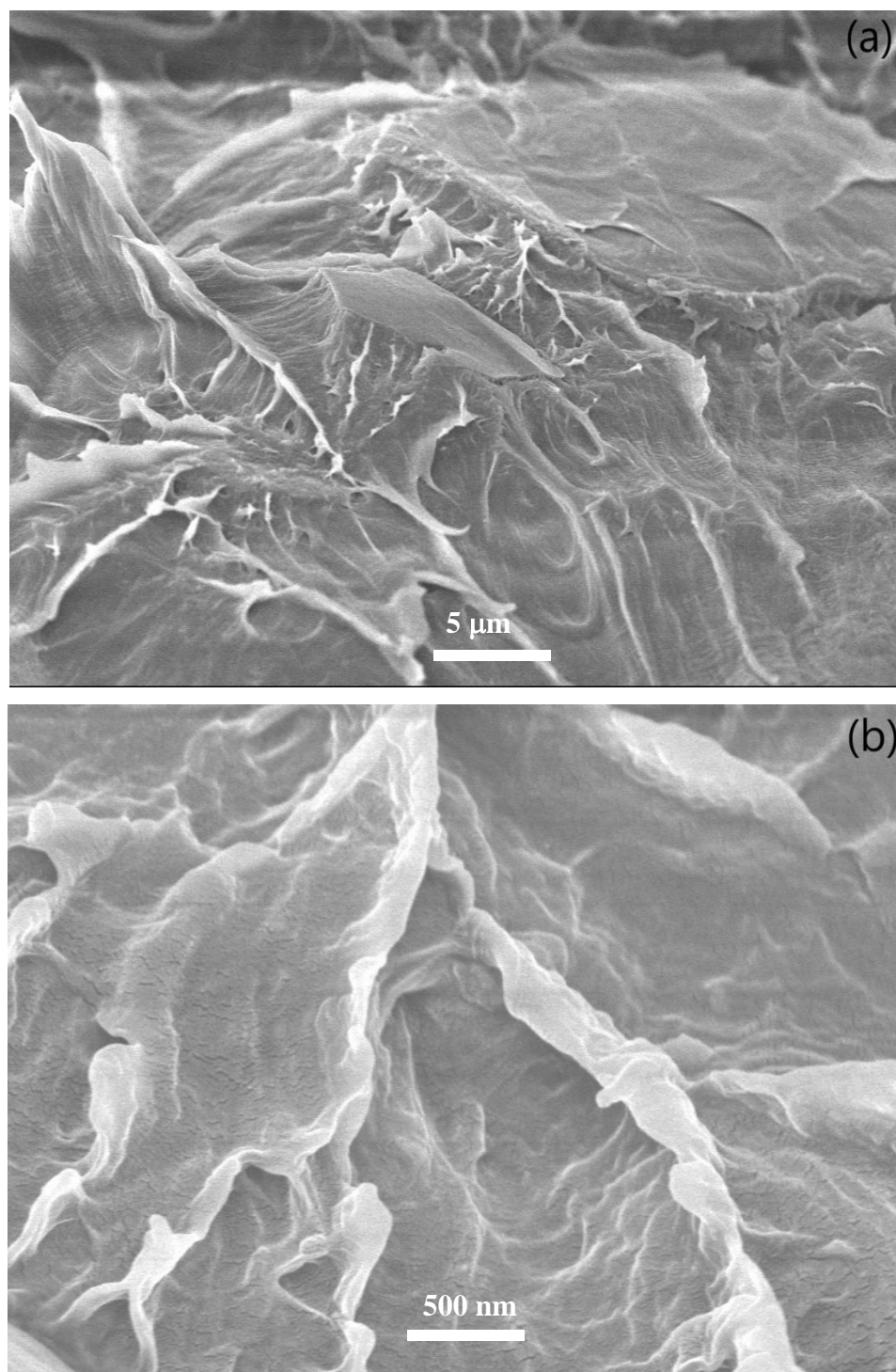


Figure 4.3: FESEM images of 1.0 wt% RGO/LDPE nanocomposite at (a) $\times 3k$ and (b) $\times 30k$ magnification.

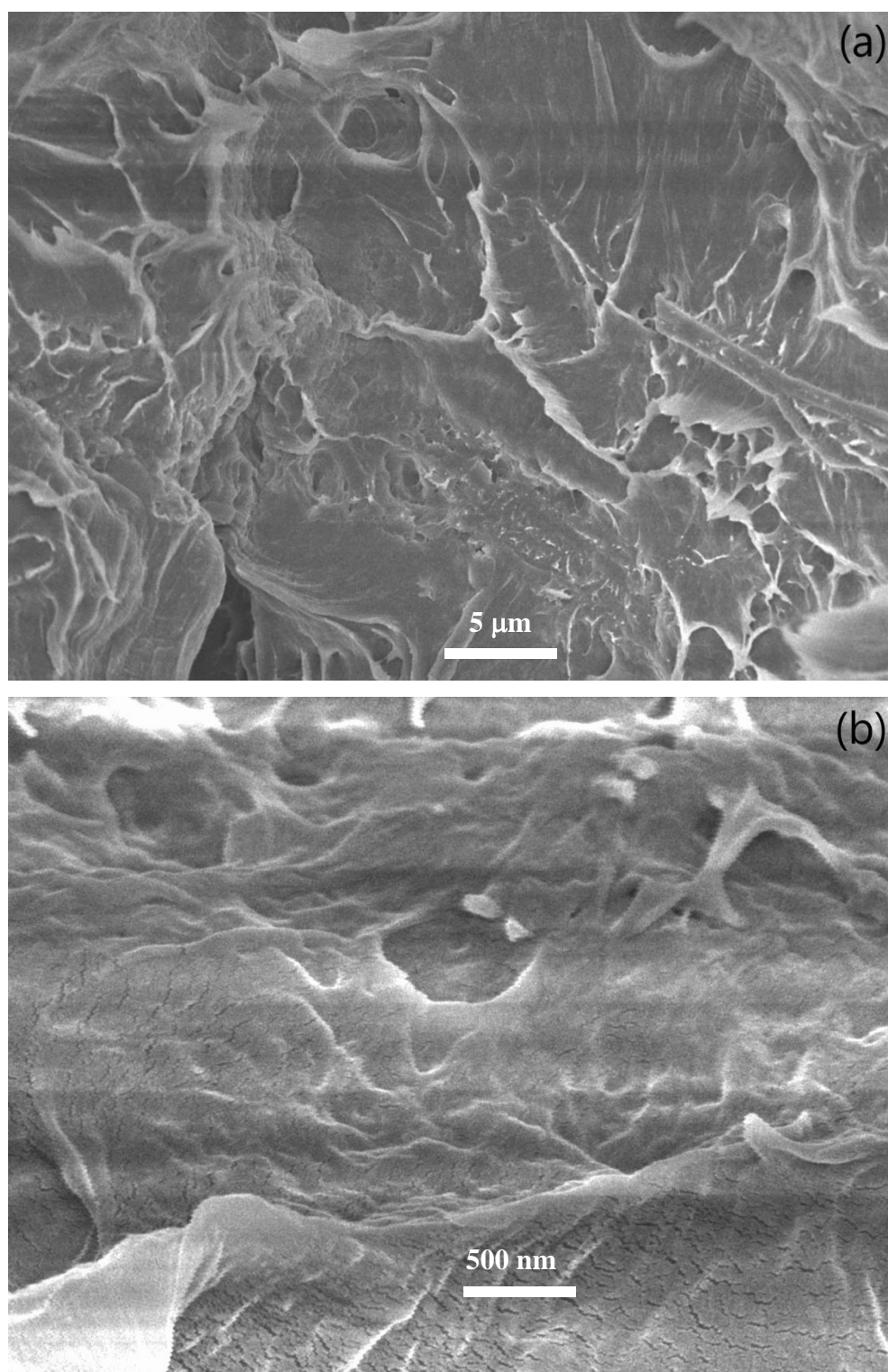


Figure 4.4: FESEM images of 2.0 wt% RGO/LDPE nanocomposite at (a) $\times 3\text{k}$ and (b) $\times 30\text{k}$ magnification.

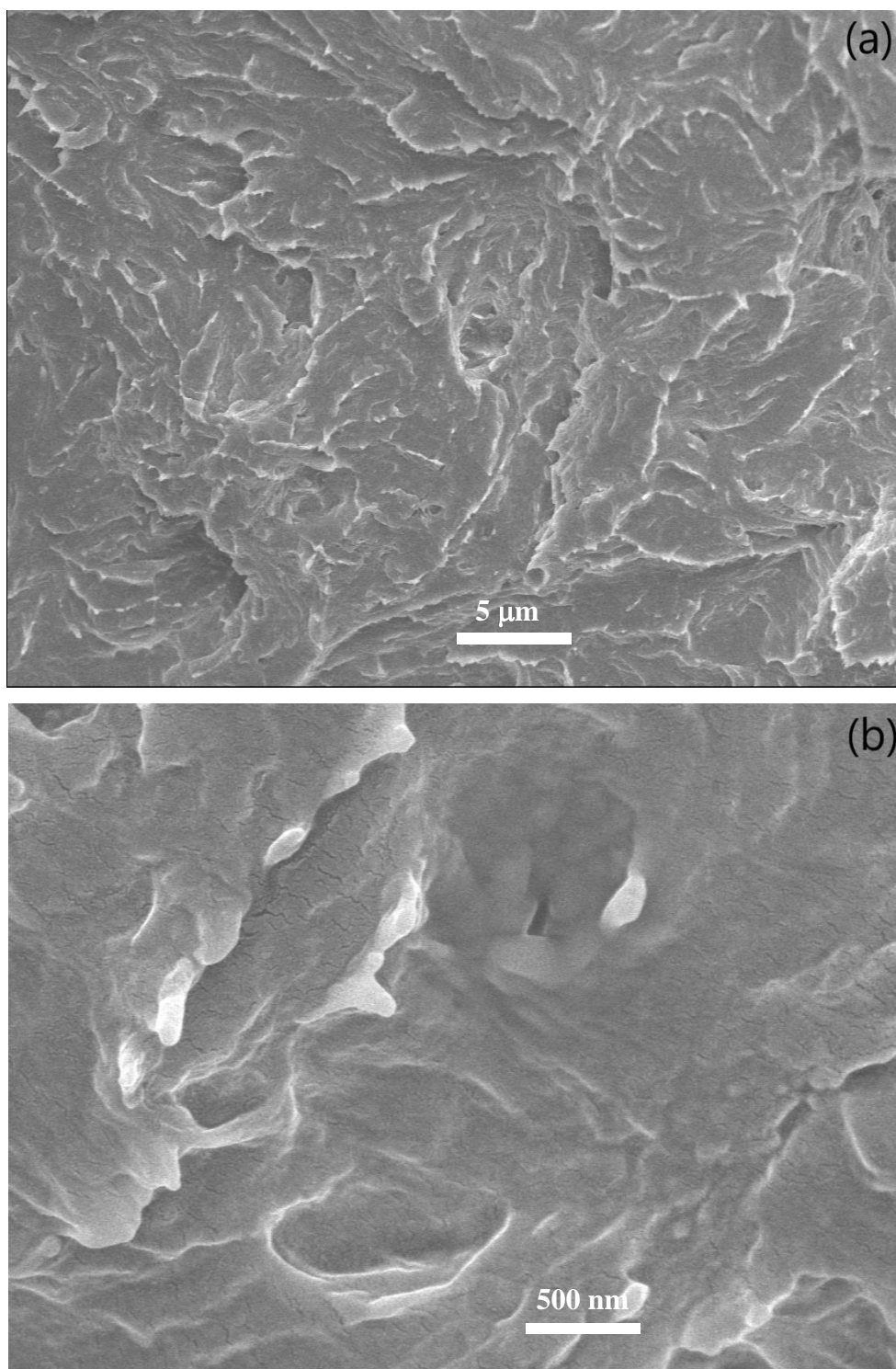


Figure 4.5: FESEM images of 3.0 wt% RGO/LDPE nanocomposite at (a) $\times 3k$ and (b) $\times 30k$ magnification.

Surface morphological investigations are done through FESEM micrograph of RGO and 0.0, 1.0, 2.0 and 3.0 wt% of RGO/LDPE nanocomposites at $\times 3k$ and $\times 30k$ magnifications, which are shown in the Figs 4.1–4.5.

FESEM observation of the RGO exhibits less agglomeration and individual wrinkled structured sheets are easily observable (Figs. 4.1a,b) as reported by the literature [51]. The devastation of orientation and the creation of macropores between the graphene sheets can be seen in the images during reduction, individually RGO sheets are unstable due to a large number of defects and dangling bonds [52]. Afterwards, for a better stability, they tend to be coupled with each other through a van der Waals interaction [53]. A large amount of gas (e.g. H_2O , CO_2 , and CO) is generated and evaporated, resulting in the interior spaces and gaps [54]. The morphology and particle size of as synthesized RGO/LDPE nanocomposites are revealed by FESEM analysis and are shown in the Figs. 4.2–4.5. The RGO shows typical 2D sheet like nanostructure with wrinkled surface or edges (Fig. 4.1) and pure LDPE shows the agglomerated nanostructure (Fig. 4.2). The composites with low loading of RGO have the similar morphology with the pure LDPE. The appearance of island-like regions in the composites with relatively higher loading of RGO indicates the presence of RGO in LDPE which are revealed as wrinkled structure. In addition, the composites with higher loading of RGO exhibited a darker contrast. The dark-contrast regions may contain wrinkled RGO sheets and a more amount RGO as stated by Jing et al. [8]. From the above observations it can be said that the further incorporation of RGO will increase the dark contrast region which expressed the presence of RGO in LDPE.

4.2 Elemental Analysis

4.2.1 Energy dispersive x-ray analysis (EDX)

The elemental analysis of the RGO and RGO loaded LDPE nanocomposites are studied by the EDX spectra as shown in Figs. 4.6–4.8 and elemental data are shown in the Table 4.1.

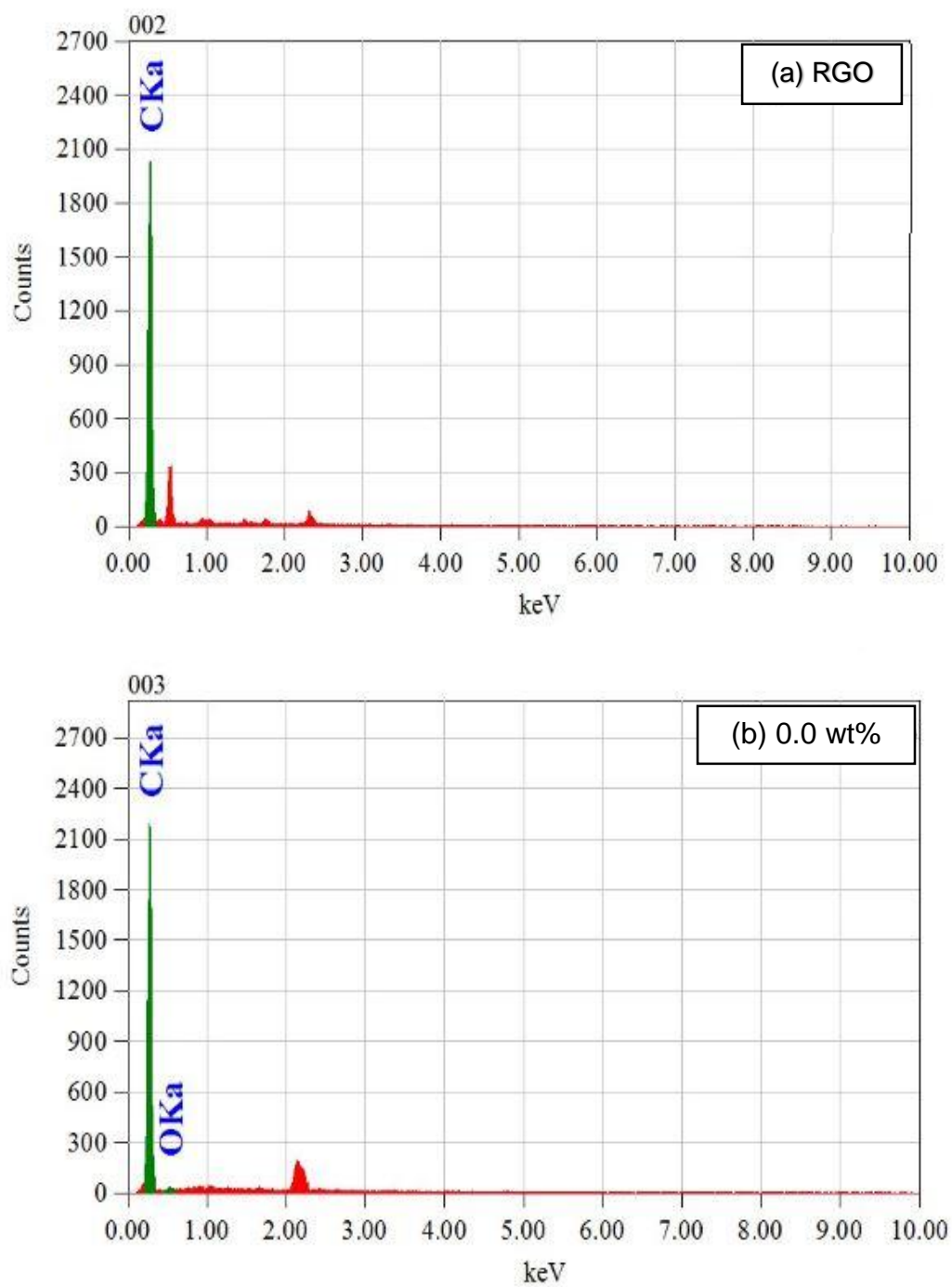


Figure 4.6: EDX spectra of (a) RGO and (b) 0.0 wt% RGO loaded RGO/LDPE nanocomposites.

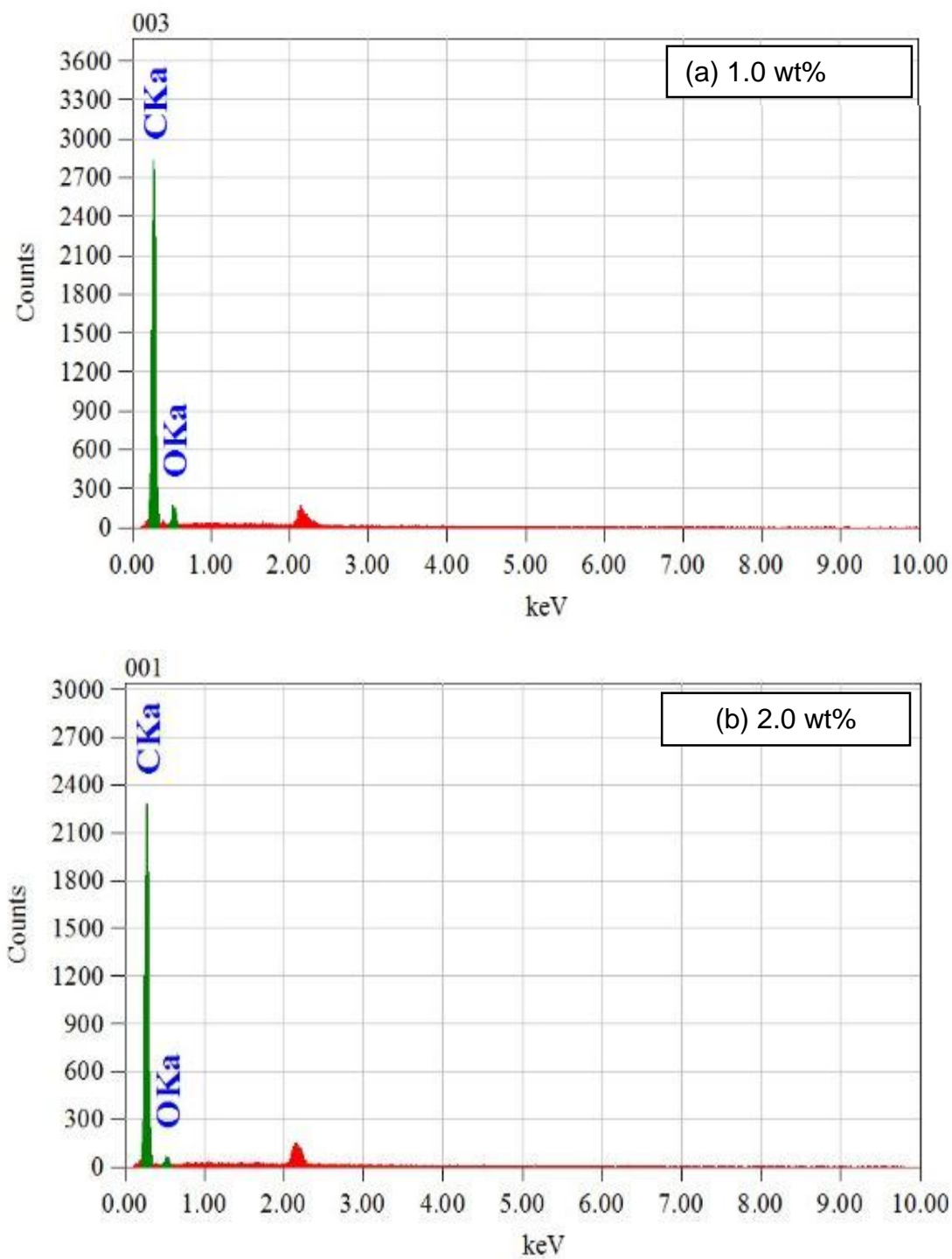


Figure 4.7: EDX spectra of (a) 1.0 wt% and (b) 2.0 wt% RGO loaded RGO/LDPE nanocomposites.

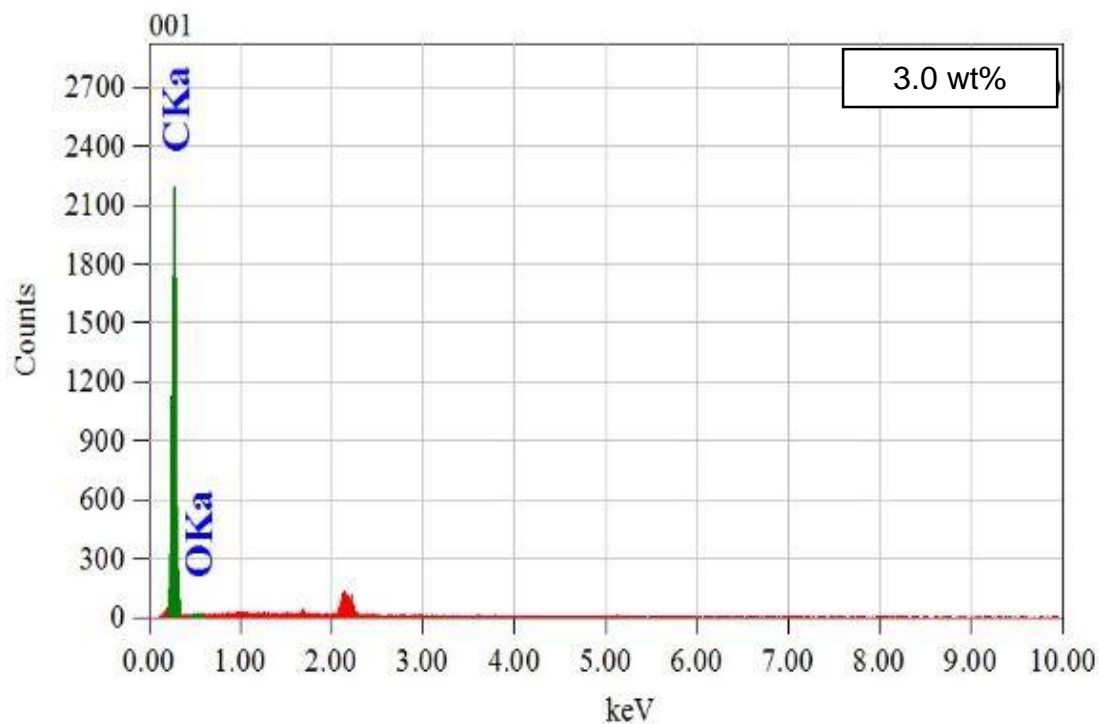


Figure 4.8: EDX spectra of 3.0 wt% RGO loaded RGO/LDPE nanocomposite.

Table 4.1: Elemental analysis data of RGO and RGO loaded LDPE nanocomposites.

Samples	Elements (C,O) in the composites with various wt%	
	C	O
RGO	100	0
0.0 wt% RGO/LDPE	98.60	1.40
1.0 wt% RGO/LDPE	86.71	13.30
2.0 wt% RGO/LDPE	97.60	2.40
3.0 wt% RGO/LDPE	98.90	1.10

The EDX spectra clearly confirmed that the presence of carbon in the RGO is 100% as expected. In the other samples it is signified that with the addition of RGO, the amount of carbon is increased proportionally. It is also expressed that the dispersion of RGO in LDPE is done properly and the presence of carbon is almost 100%.

4.3 Structural Analyses

4.3.1 X-ray diffraction (XRD) pattern

The structure analysis of RGO and RGO/LDPE nanocomposites are studied by XRD pattern as shown in the Figs. 4.9–4.10.

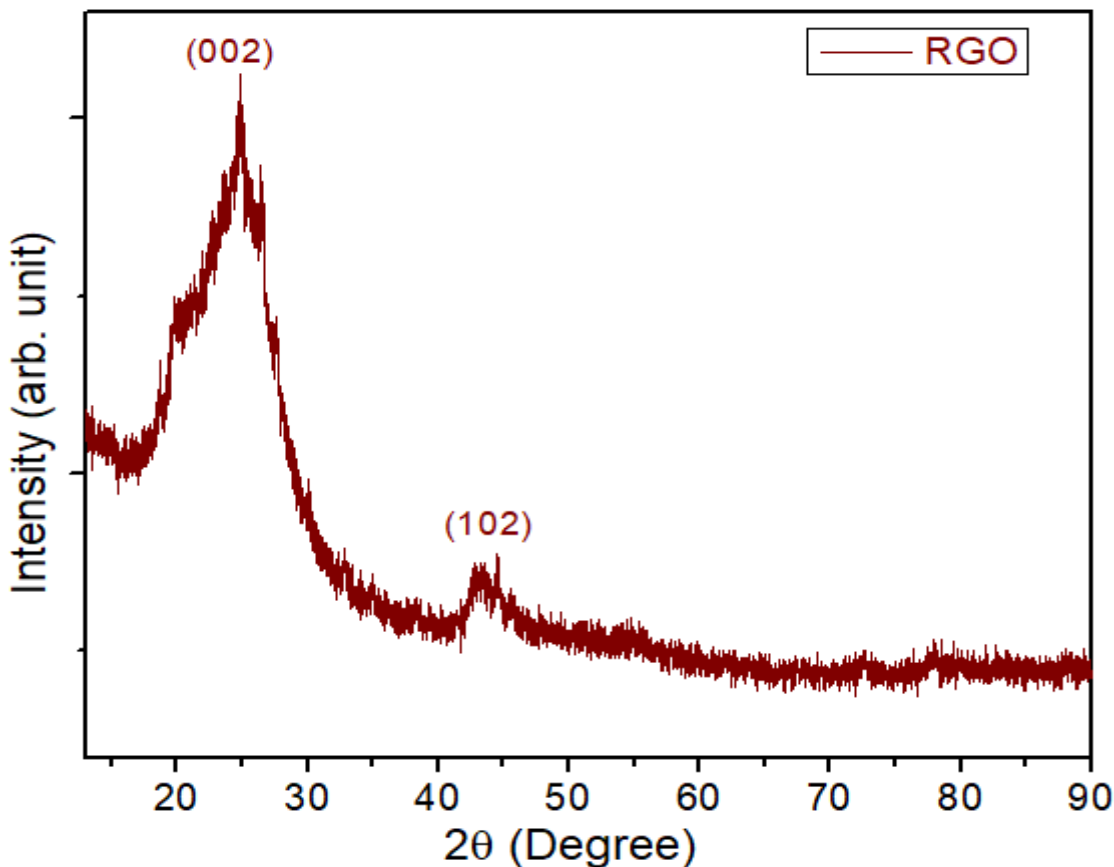


Figure 4.9: XRD patterns of RGO.

XRD measurement is used to determine the crystal structure and lattice parameter of RGO. A peak is observed at diffraction angle $2\theta = 24.8^\circ$ corresponding interlayer spacing of 0.36 nm of the planes (002). In crystalline graphite, this value is 0.34 nm and the increase of lattice spacing in RGO indicates the presence of oxygen functional groups and the broad peak is responsible for few layer of RGO sheets as reported in the literature [6, 55–57]. A small diffraction peak is also seen in the angle of 43.2° of the plane (102) of interlayer spacing 0.209 nm of RGO structure, which is completely consistent with the Bragg's equation ($2d\sin\theta=n\lambda$) that, interlayer spacing (d) is decreased with the increase of diffraction angle (2θ) in which the 2θ is increased due to the removal of oxygen functional group as similar

to the literature [58]. The decrease in interlayer spacing for RGO is resulted by stacking of graphene sheets due to the Van der Waals interaction forces between the layers [59].

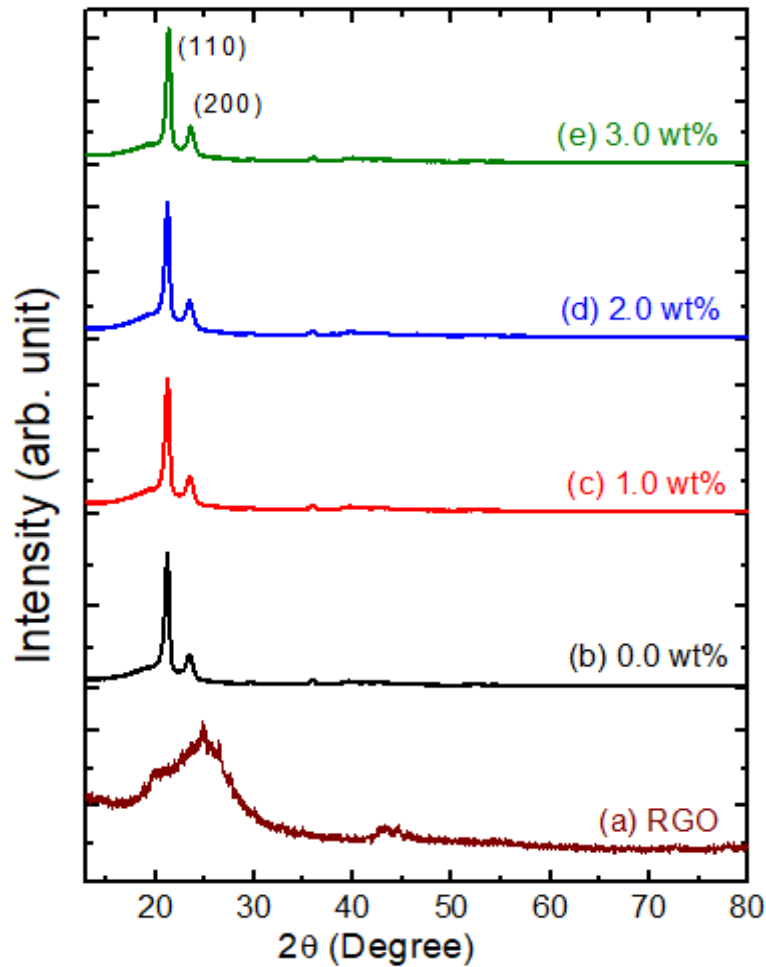


Figure 4.10: XRD patterns of (a) RGO and (b–e) RGO loaded RGO/LDPE nanocomposite.

Now the crystallographic structure of RGO based LDPE nanocomposites are shown in the Fig. 4.10, which is investigated by XRD analysis. The XRD pattern of 0–3 wt% also shows two peaks at 21.3° and 23.3° of planes (110) and (200) in the corresponding interlayer spacing of 0.42 and 0.38 nm respectively, which are very compatible with the published result [7]. Further the crystallite size (D) of the composite is calculated by using the Scherrer formula,

$$D = \frac{0.89\lambda}{\beta \cos\theta} \dots \dots \dots (4.1)$$

Where, λ , β and θ are the wavelength, full width half maximum (FWHM) and diffraction angle, respectively.

Table 4.2: XRD measurement data of RGO and RGO loaded RGO/LDPE nanocomposites.

Samples	Crystallite size (nm)at 2θ
0.0 wt%	73
1.0 wt%	27
2.0 wt%	73
3.0 wt%	85

After incorporation of RGO in the pure LDPE the crystallite size became very low at 1.0 wt% and it is gradually increased with the further increase of RGO as shown in the table 4.2. Therefore it summarizes that the addition of RGO in higher concentration helps to improve the crystallite size of the composite, which are similar to the literature [60].

4.3.2 Fourier-transform infrared spectroscopy (FTIR)

The mid-range IR absorption is used to detect the functional groups of organic compounds. The FTIR spectra of pure LDPE and 1–3 wt% of RGO loaded LDPE nanocomposites are shown in the Fig. 4.11.

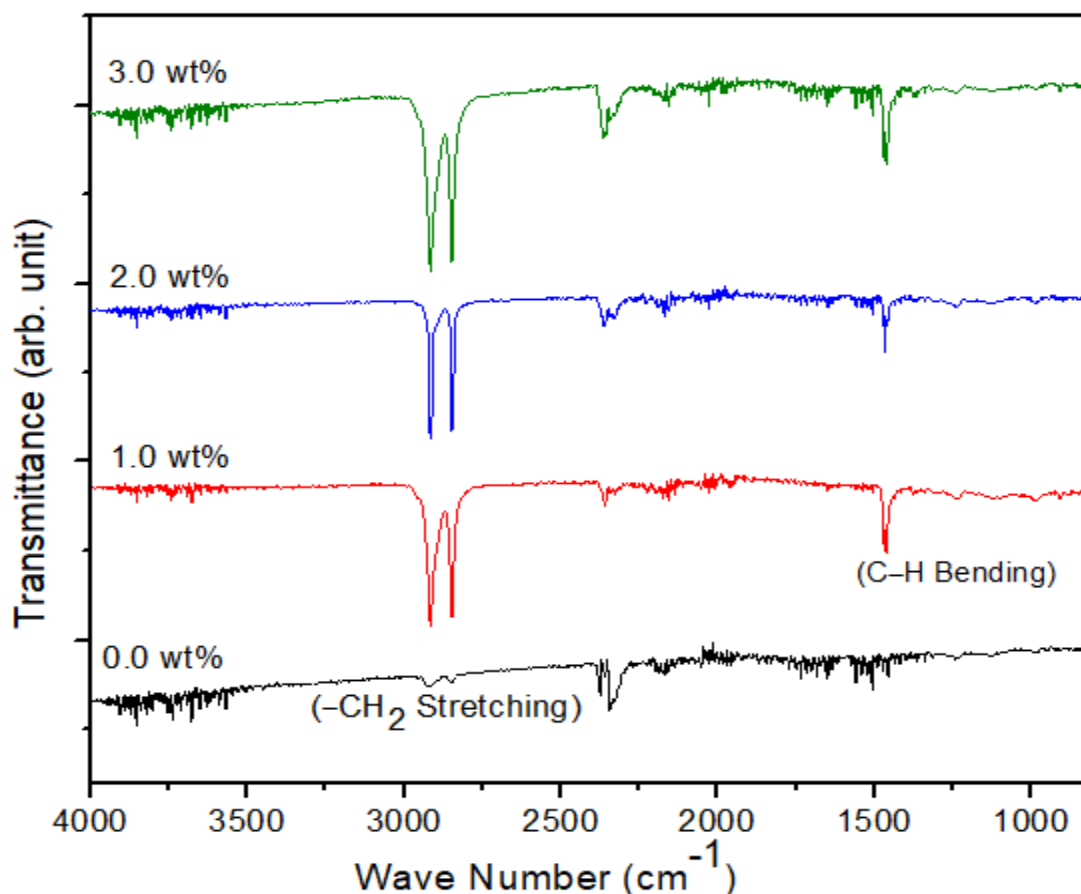


Figure 4.11: FTIR spectra of pure LDPE and RGO loaded RGO/LDPE composite.

In covalent bonds the atom rotates and vibrates around their bonds and the bonds are bend, contracted and stretched by dint of the rotational and vibrational force. The spectral image exhibits that there is no significant absorption peaks in the pure LDPE. In the concentration of 1.0, 2.0 and 3.0 wt%, the significant absorption peaks are appeared in the spectra corresponding to 1465, 2850 and 2914 cm^{-1} . In 1465 cm^{-1} the bonds are twisted in their angular direction and a peak is detected to attribute the bending absorption of C–H bond. Moreover, two significant peaks are observed at 2850 and 2914 cm^{-1} respectively. In this region the bonds are stretched and the stretched absorptions are attribute to $-\text{CH}_2$ compound, as reported by Jing et al. [8]. These spectra shows that there are structural changes due to the variation of RGO as a filler agents in the LDPE matrix and the chemical structure of the composites differ to the pure LDPE structure.

4.4 Thermal Analyses

4.4.1 Thermogravimetric/derivative thermogravimetric (TG/DTG) analysis

The TGA and DTG treatment is used to investigate the thermal stability of material. Here pure LDPE and RGO/LDPE nanocomposite samples are performed in N_2 environment.

The characteristic curves for this treatment are shown in Fig. 4.12.

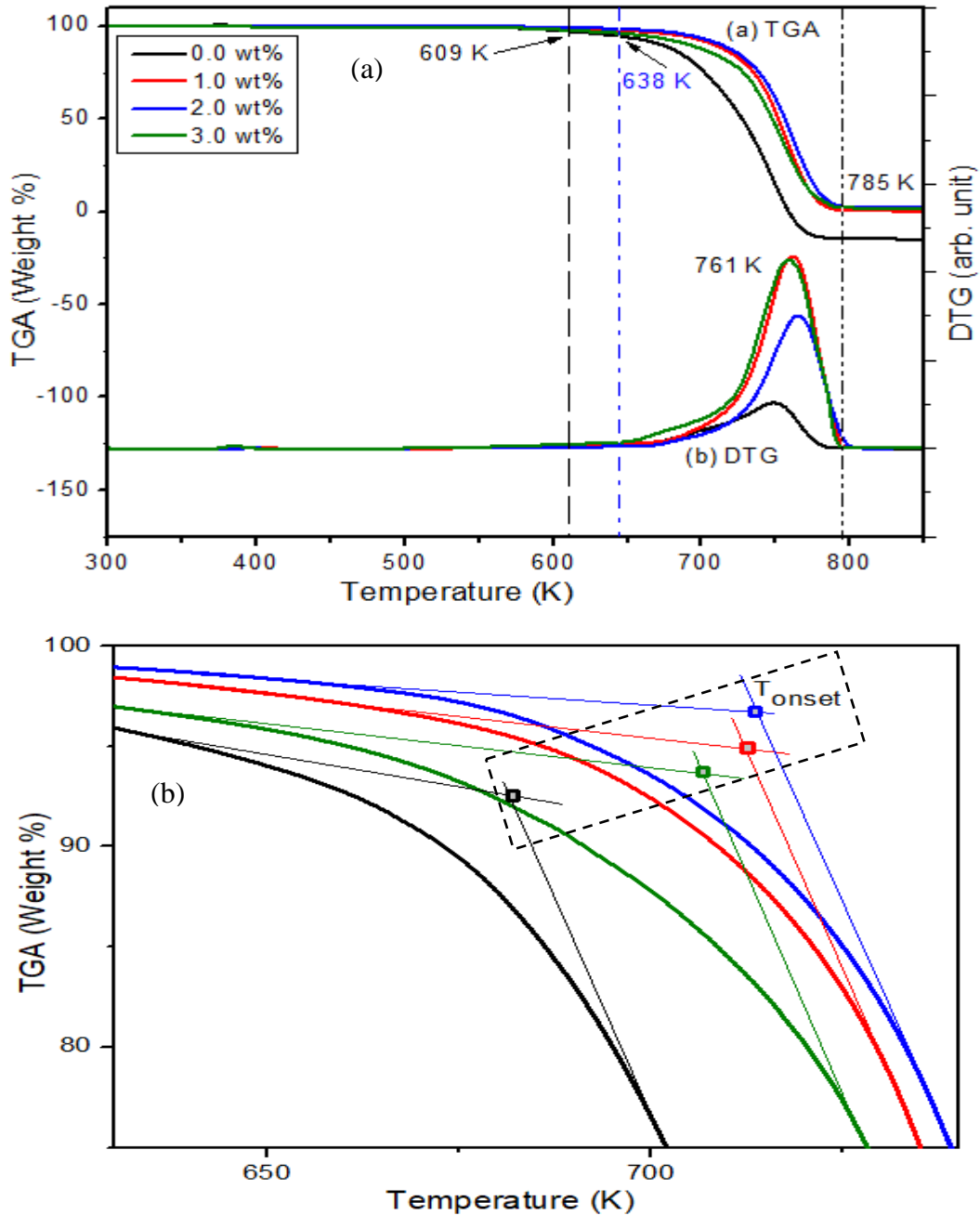


Figure 4.12: (a) TG/DTG curves of pure LDPE and RGO loaded RGO/LDPE nanocomposites and (b) Highlight of T_{onset} .

This results show that the initial degradation temperature of pure LDPE is 609 K and it is shifted to 638 K for 1–3 wt% of RGO loaded LDPE nanocomposites (Table 4.3).

Table 4.3: TGA measurement data of pure LDPE and RGO/LDPE nanocomposites.

Sample	Initial degradation		Final degradation		
	Temp. (K)	Weight loss (%)	Temp. (K)	Weight loss (%)	T _{onset} (K)
0.0 wt%	300–609	9.98	609–785	100	680
1.0 wt%	300–638	3.72	638–785	99.15	712
2.0 wt%		2.76		97.28	714
3.0 wt%		6.83		97.77	707

In the initial degradation region, very small amount of material is lost due to the presence of moisture content. No DTG peak is seen in this corresponding region. The maximum decomposition has become in the next region and it lasts till 785 K. In this region the Pure LDPE is totally burned and several portion of the composite have been burned. The 3.0 wt% gives anomalous result which may be due to the coagulation of foreign particle RGO for more concentration. The corresponding DTG characteristic curve shows a peak at 761 K in this region, which represents the maximum decomposition. The degradation temperature is shifted to higher order due to the addition of RGO in LDPE and minimum weight is lost in this region as reported by the literature [61, 8]. Therefore, RGO helps to improve the stability of LDPE in thermal applications.

4.5 Mechanical Strength

The mechanical characterization of the pure LDPE and 1–3 wt% of RGO loaded LDPE nanocomposites are carried out by universal testing machine (UTM) as shown in Fig. 4.13. The specimen is cut into desired shape for this test where gauge length = 30 mm, width = 12 mm and thickness = 4 mm.

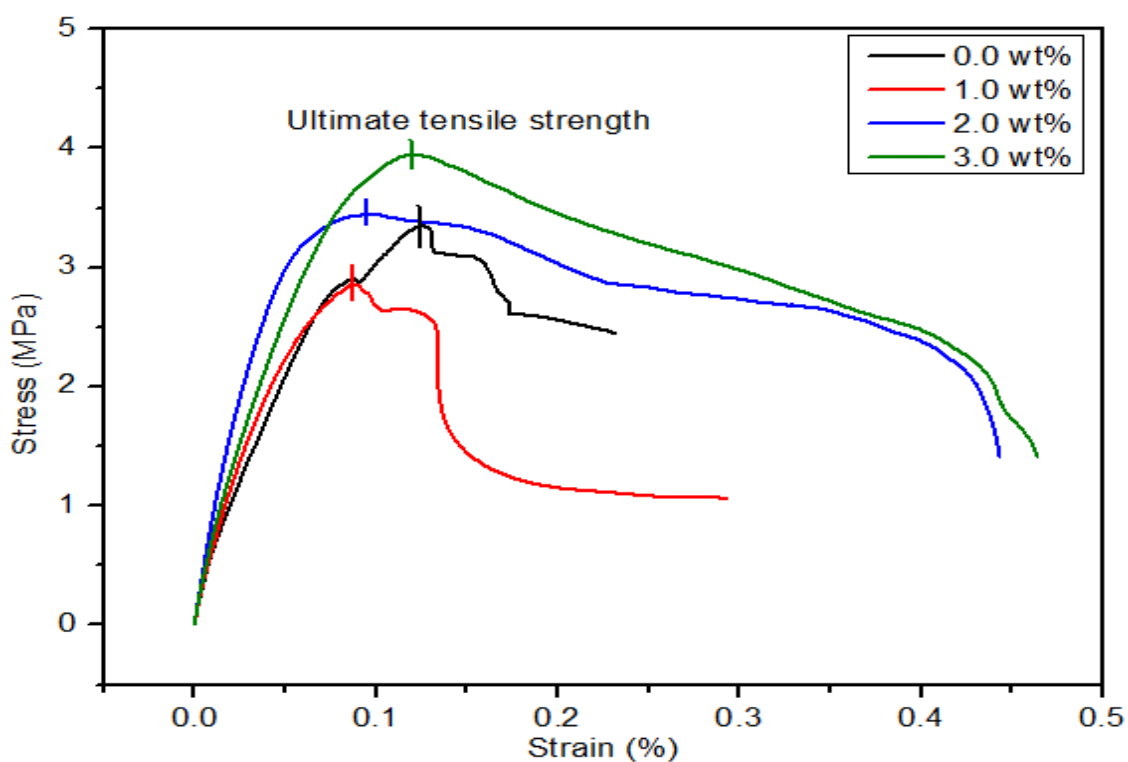


Figure 4.13: Stress–strain curves for pure LDPE and RGO loaded LDPE nanocomposite.

In this investigation, three parameters are observed such as, ultimate tensile strength (UTS), elongation at break (EB) and Young modulus (Y). The highest force per unit area is known as ultimate tensile strength (UTS). Initially it followed the Hook's law [62] before UTS point, which is known as elastic region. These results also reveal that the UTS value for pure LDPE is relatively low and it is increased with the increase of filler (Table 4.4), which is compatible to the literature [7, 63].

Table 4.4: Mechanical testing data of RGO/LDPE nanocomposites.

Samples	Ultimate Tensile Strength (MPa)		Elongation at break (%)	Young Modulus (MPa)
0.0 wt%	3.34	5.2 [7]	23.15	121.93
1.0 wt%	2.86		29.3	157.27
2.0 wt%	3.45		44.33	130.39
3.0 wt%	3.95	6.5 [7]	46.41	134.09

The Young Modulus and elongation at break of the composites are also increased with the increase of RGO concentration in pure LDPE, which are similar to the result reported by Carotenuto et al. [64]. An exception arises in 1.0 wt% where the anomaly result is revealed. This anomaly result may be due to the improper dispersion of filler or creation of porosity during composite fabrication. This results expressed that the incorporation of carbon based filler upgrades the mechanical properties of LDPE that can be a great application. However the tensile strength calculated here is slightly smaller than the actual value than that of pure LDPE, which may be due to the creation of void during composite fabrication.

4.6 Electrical Properties

To investigate the electrical properties of polymer nanocomposite is the important and very critical characterization all of the properties. Several scientists have been working for it and tried to improve this properties for a long time. The notable electrical properties such as current density, conductivity, dielectric constants, etc. are discussed here.

4.6.1 DC current density

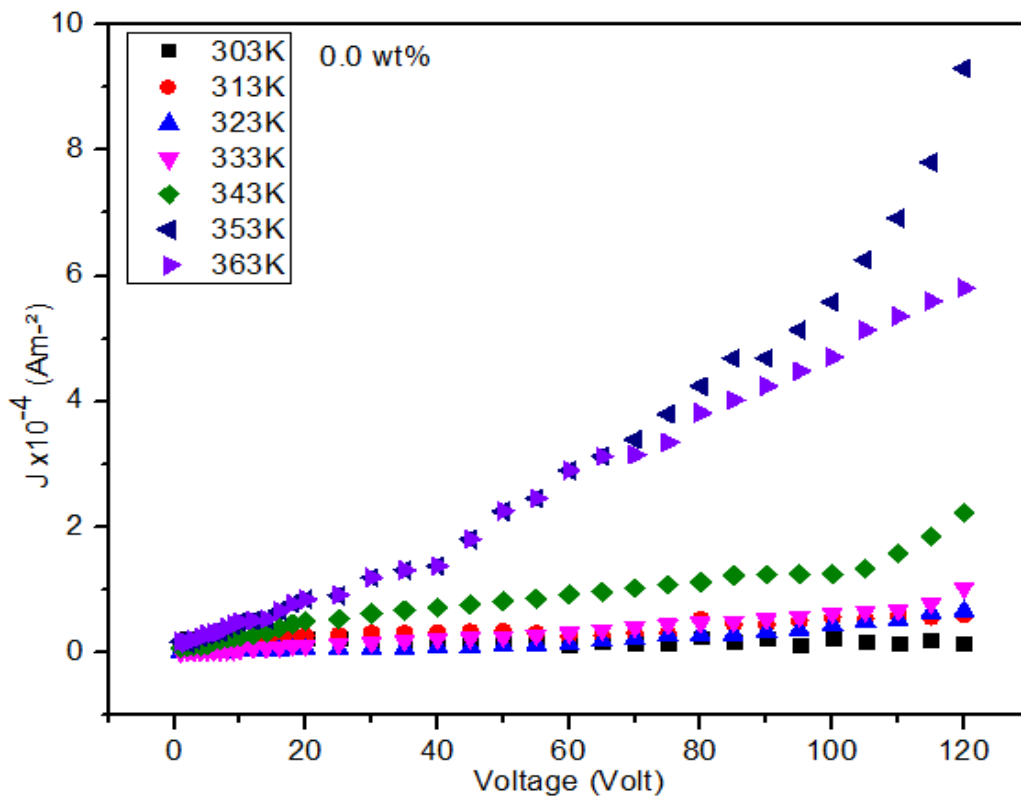


Figure 4.14: J–V characteristic curves of pure LDPE at different temperature.

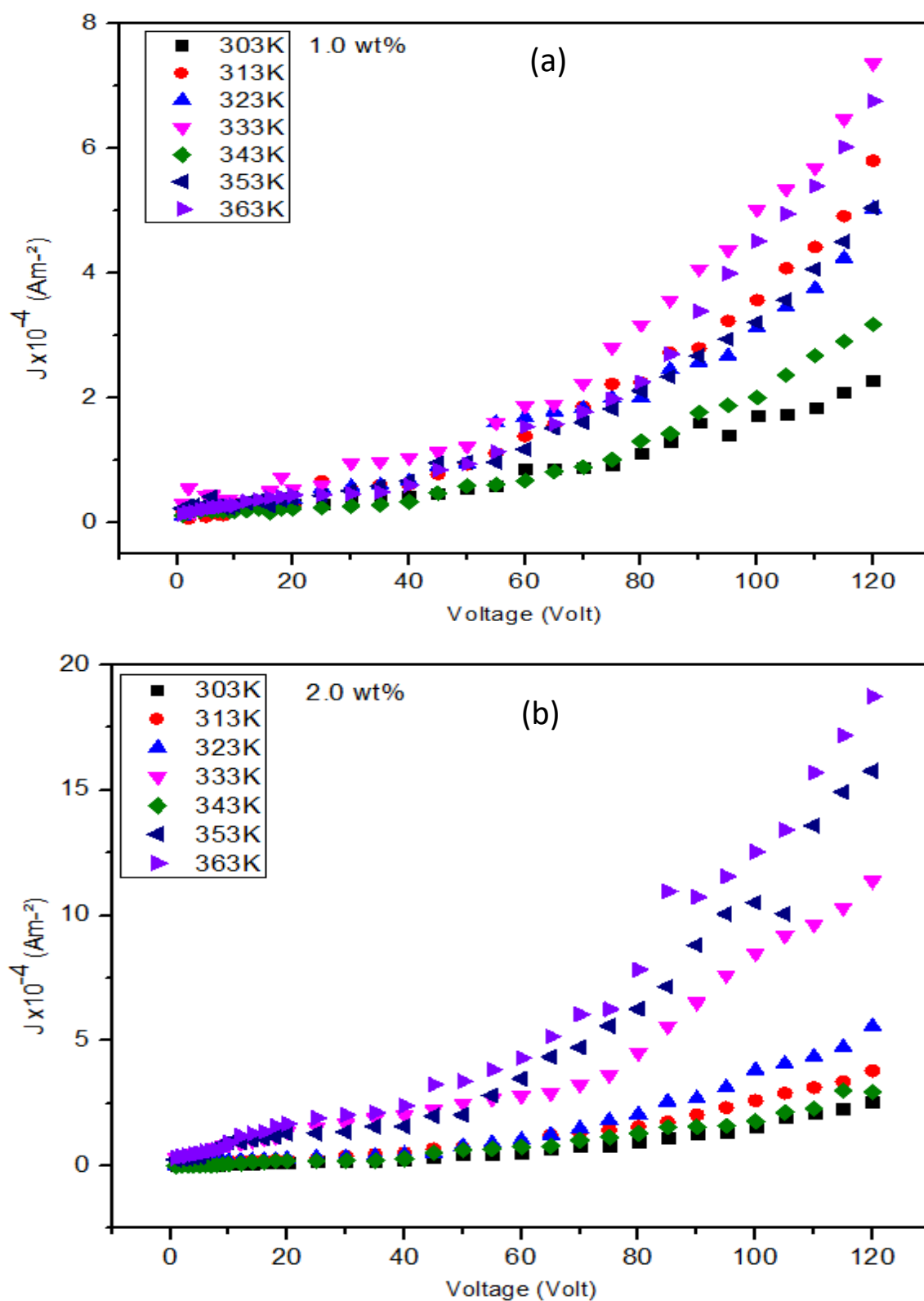


Figure 4.15: J–V characteristic curves of (a) 1.0 wt% and (b) 2.0 wt% of RGO loaded RGO/LDPE nanocomposite at different temperature.

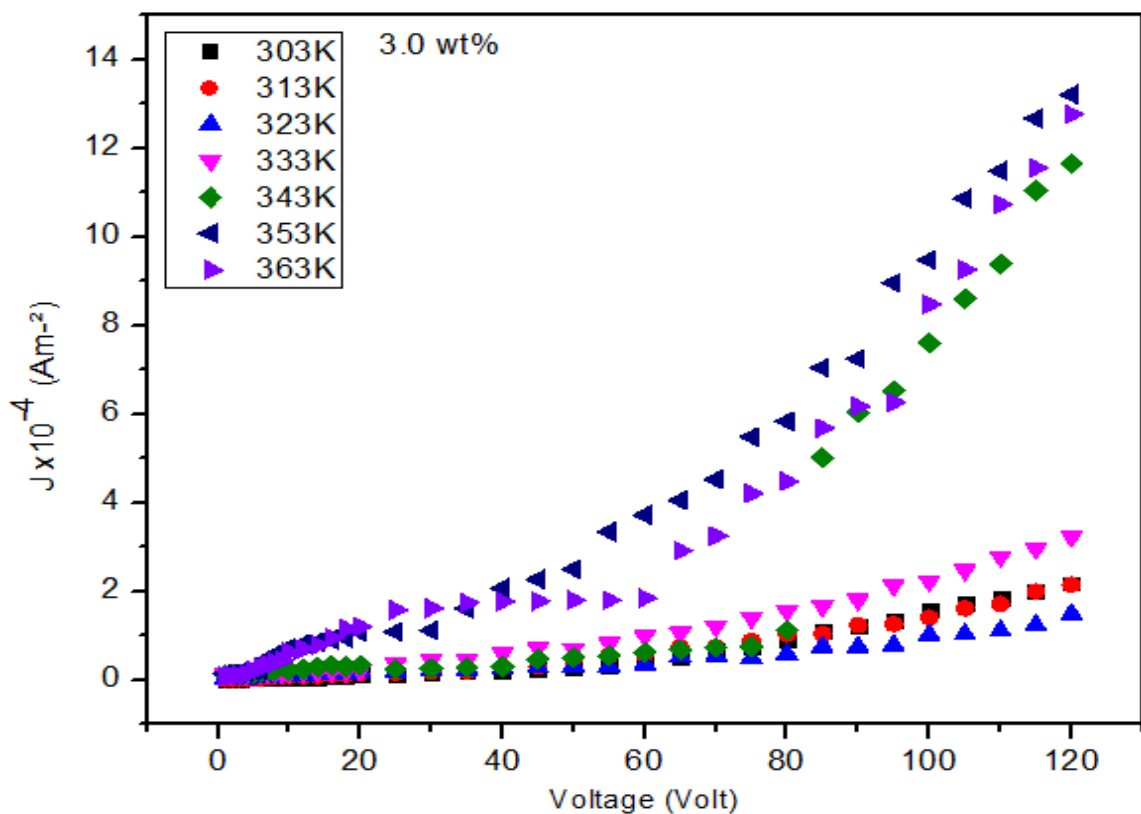


Figure 4.16: J–V characteristic curves of 3.0 wt% of RGO loaded RGO/LDPE nanocomposite at different temperature.

The current density versus voltage (J–V) at different wt% of RGO characteristic curves for pure LDPE and RGO/LDPE nanocomposites are shown in the Figs. 4.14–4.16. These study revealed that the current density is almost zero at pure LDPE and it increases gradually but after a certain concentration suddenly it decreases at 3.0 wt%, it may be due to the coagulation of RGO when much amount is mixed with LDPE.

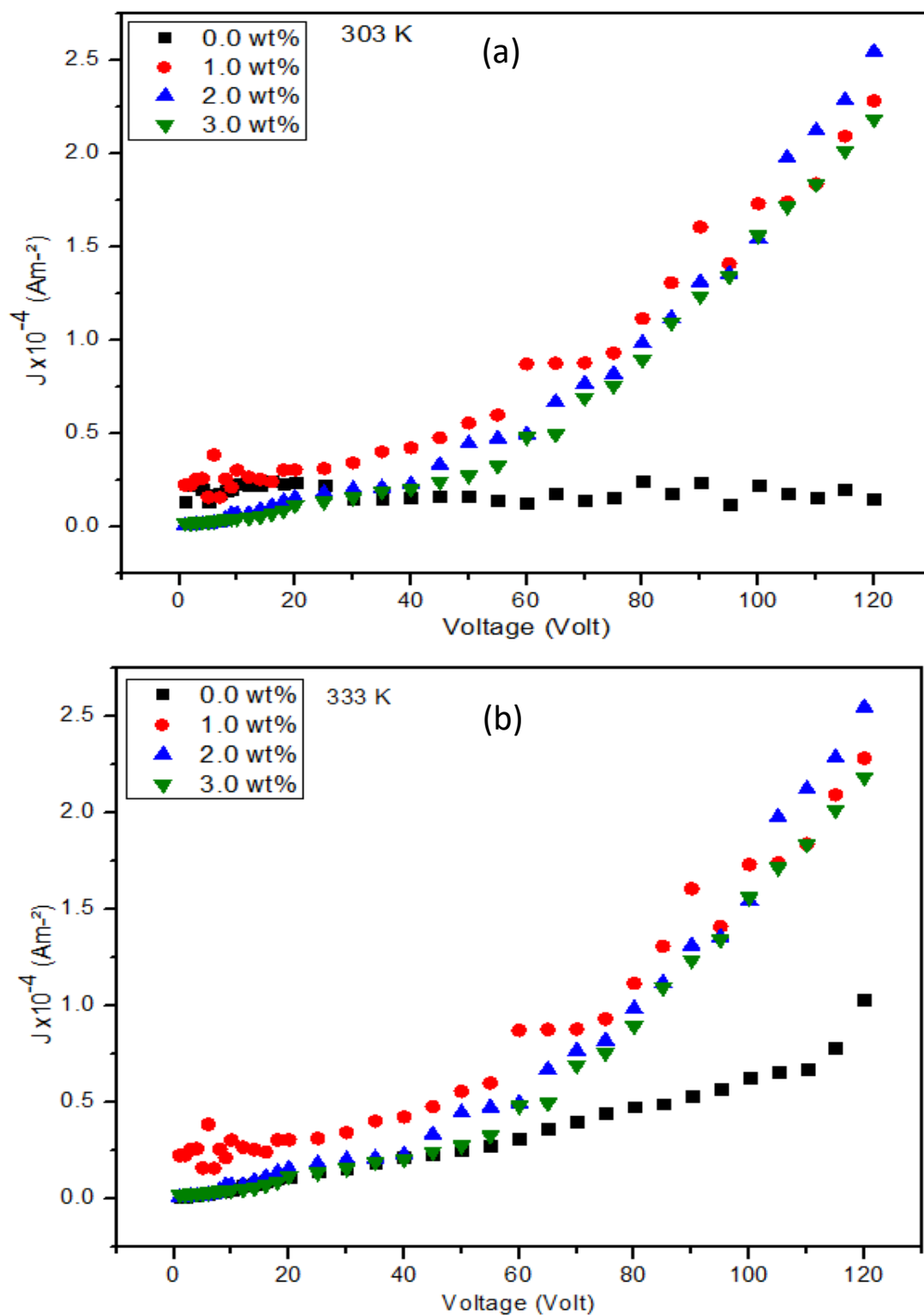


Figure 4.17: J–V characteristic curves of RGO loaded RGO/LDPE nanocomposite at temperature (a) 303 K and (b) 333 K.

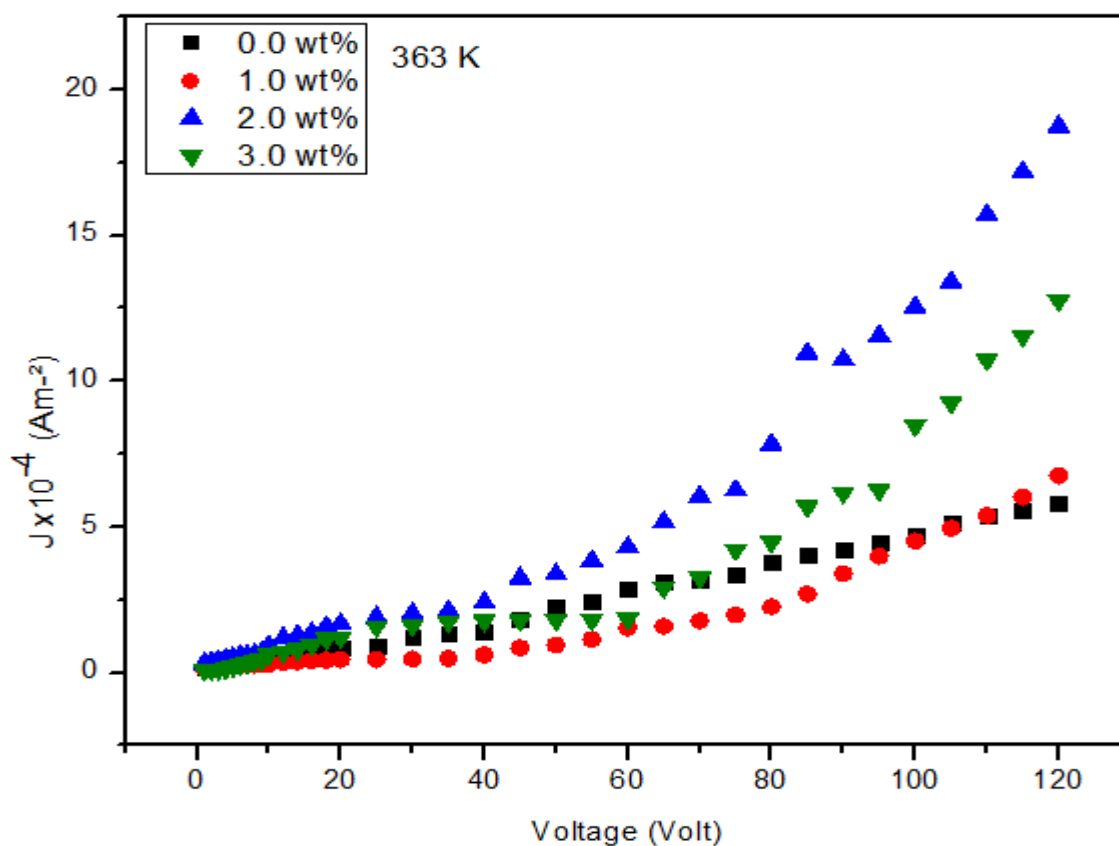


Figure 4.18: J–V characteristic curves of RGO loaded RGO/LDPE nanocomposite at temperature 363 K.

And the current density (J) versus voltage at different temperature are shown in the Figs. 4.17 –4.18. It reveals that the current density is almost zero at room temperature and it gradually increases due to increases of temperature. The properties of increasing current density with respect to increasing temperature is very consistent with the semiconducting nature of material.

4.6.2 DC electrical conductivity

The temperature dependent electrical conductivity of pure LDPE and 1–3 wt% RGO loaded RGO/LDPE nanocomposite and the conductivity with various temperature is shown in Fig. 4.19.

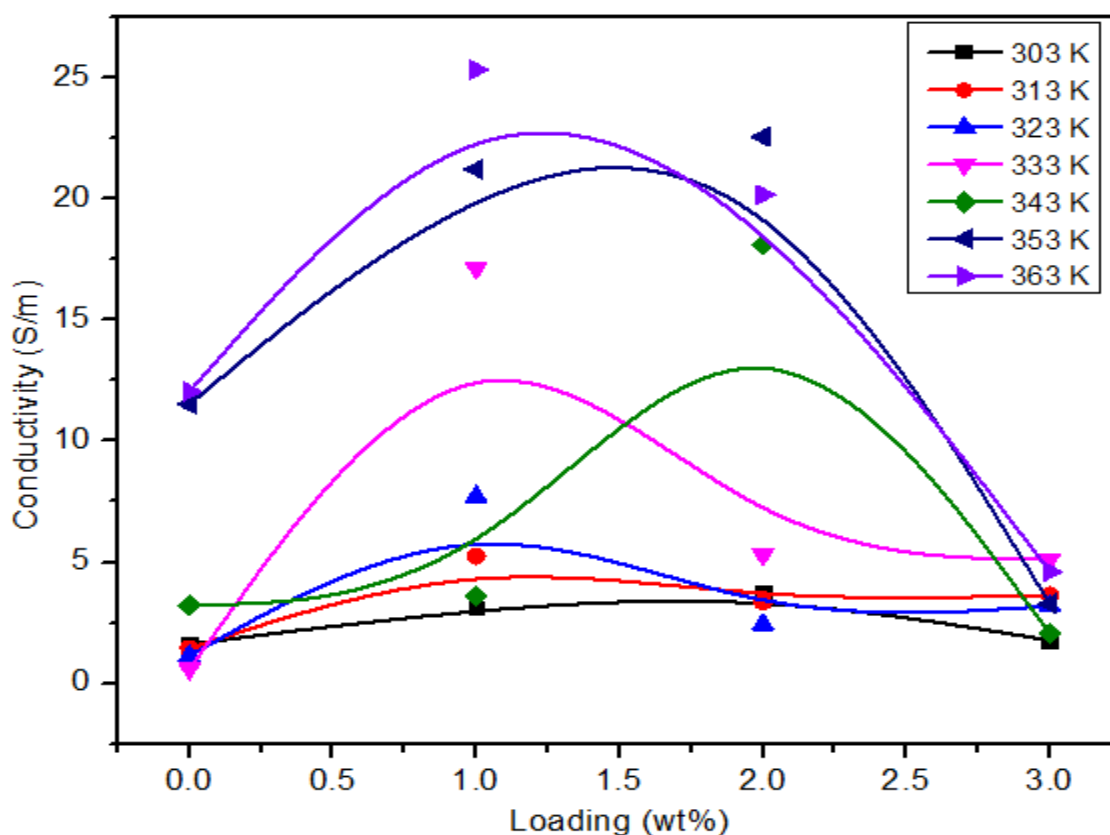


Figure 4.19: DC conductivity with respect to different wt% of RGO in RGO loaded RGO/LDPE nanocomposite at different temperature.

This image is revealed that the dc electrical conductivity is increased with the increase of temperature. And for concentration, the pure LDPE reveals insulating nature because of its low amount of free electron mobility. The incorporation of RGO in the LDPE matrix exhibits substantial improvement of electrical conductivity of the nanocomposite due to dispersion of RGO in LDPE. Moreover the electrical conductivity increases initially with wt% and it becomes highest at 1.0 wt% and consequently at 2–3 wt% it decreases gradually. The RGO gets coagulated due to incorporation of high wt% of it in LDPE and thus the conductivity decreases in the higher wt% of RGO/LDPE nanocomposite.

4.6.3 Dielectric properties

The frequency dependent dielectric constant and dielectric loss factor of pure LDPE and 1–3 wt% of RGO/LDPE nanocomposite at room temperature are shown in the Fig. 4.20.

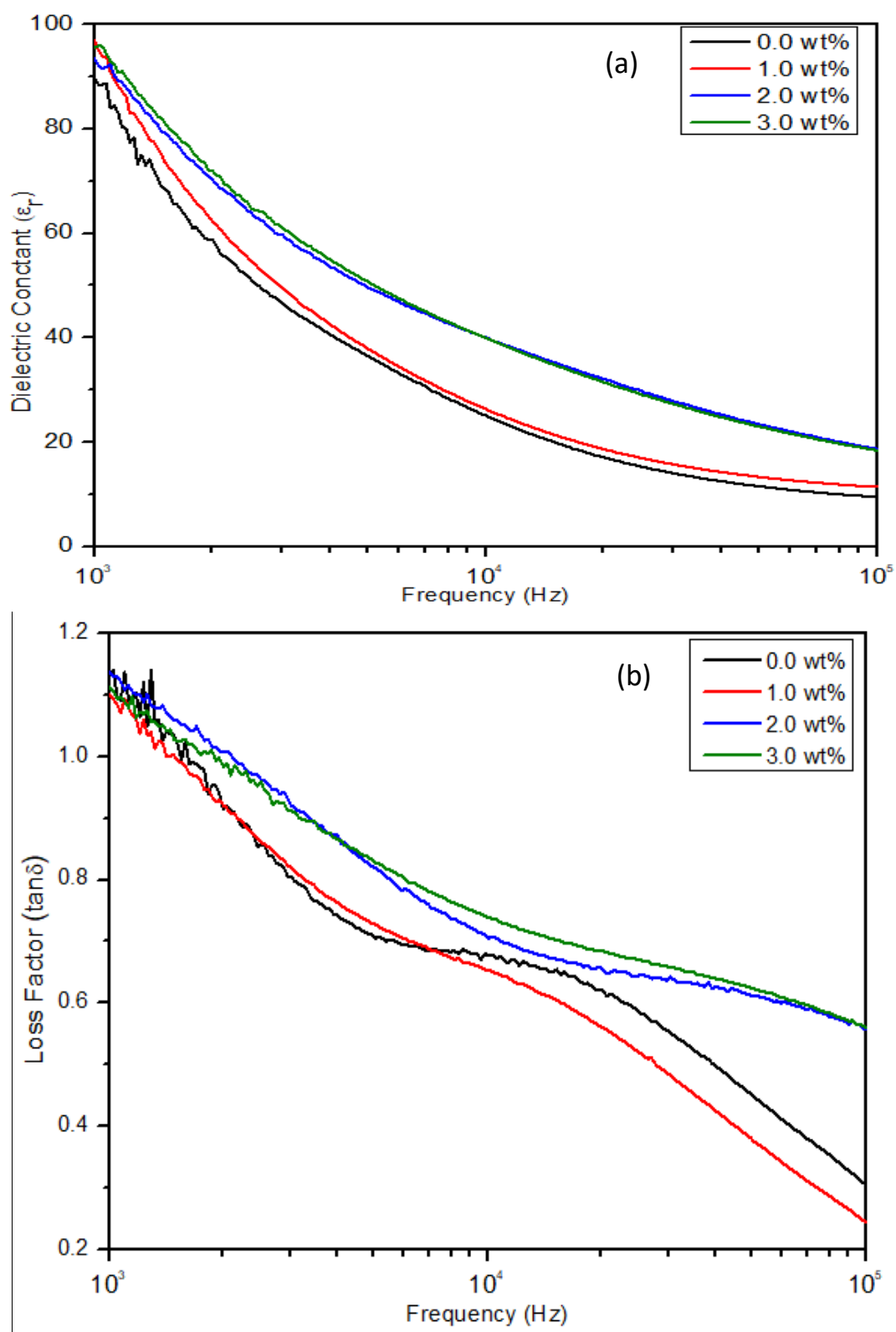


Figure 4.20: Graphical representation of frequency dependent (a) dielectric constant and (b) dielectric loss.

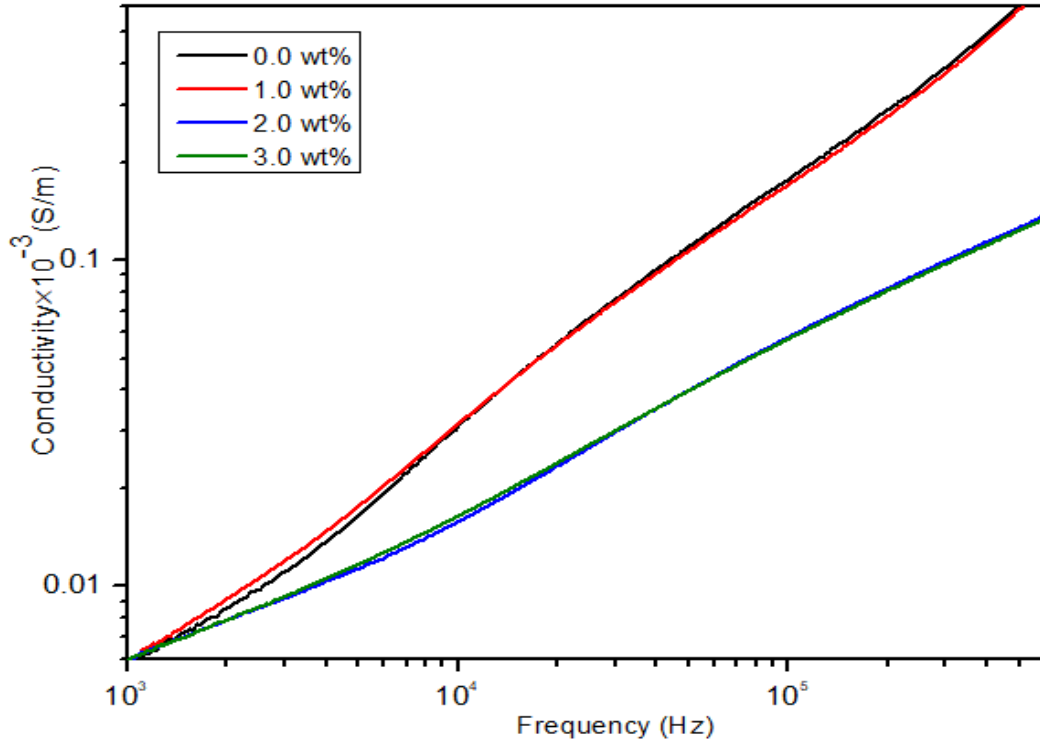


Figure 4.21: Graphical representation of frequency dependent electrical conductivity.

The dielectric properties is the molecular properties which creates polarization inside the materials when it is subjected to an external electric field. The polarization has two parts such as, real and imaginary. The real part is for dielectric constant and the imaginary part is for dielectric loss factor. It is observed that the dielectric constant and dielectric loss factor is exponentially decreased with the increase of frequency. In low frequencies the dipoles are oriented and in the higher frequencies the orientation of the dipoles are reduced thus the dielectric constant is decreased at higher frequencies. The good dielectric constant and low dielectric loss factor is the significant properties of any dielectric materials [65]. On the other hand, the dielectric constant of pure LDPE is relatively low and started to increase with the increase of filler wt%. Now the image (Fig. 4.21) reveals the frequency dependent electrical conductivity. The frequency dependent electrical conductivity reveals that the conductivity is increased with frequency. It also shows that the conductivity is high at lower filler wt% and its decreases with the increase of filler wt%. This result directs that the electrical insulation level of the composites is enhanced by the addition of RGO. Jing et al. [8] explained that the addition of more RGO coagulated itself and introduced deep

traps in the composites, thus the free electron mobility is decreased with increase of filler agents which reduced the electrical conductivity of the composites. The decreased electrical conductivity of RGO/LDPE nanocomposite show that it is a perfect insulating material in dielectric applications.

CHAPTER 5

CONCLUSIONS

5.1 Conclusions

Polymer materials are very important for modern science and technology, but they have some limitations. To overcome these limitations the properties of the materials should be improved by incorporating proper filler agent. In this thesis it is tried to improve the electrical, thermal and mechanical properties of pure LDPE by incorporating the wonder material graphene. Various methods have been performing to incorporate the filler with the matrix material but extrusion molding method has been chosen here to avoid the laborious functionalization of reduced graphene oxide (RGO).

At the very beginning, an extrusion molding machine (EMM) is locally fabricated where the necessary components are collected from a local market with very low cost. Then reduced graphene oxide (RGO) is synthesized from graphite powder and low density polyethylene (LDPE) pellets is collected from a local market market. The final RGO/LDPE nanocomposites are fabricated by using the EMM and the composites are investigated through following characterizations:

The surface morphological investigations of the pure LDPE and RGO loaded RGO/LDPE nanocomposite are studied by FESEM analysis. The FESEM pattern of RGO is revealed as wrinkle structure of 2D graphene sheets and the pure LDPE is revealed as agglomeration structure. The pattern of low concentration of RGO is similar to the pure LDPE. The surface morphological variation is clearly detectable at the higher concentration (3.0 wt%) of RGO where the wrinkle structure, island like region and darker spots are responsible for the presence of RGO in the pure LDPE.

Structural analysis of the RGO, pure LDPE and RGO/LDPE nanocomposite is studied by XRD patterns and the results explained that the crystallite size of the nanocomposite is increased by the incorporation of RGO.

The chemical composition of the composites are studied by the FTIR analysis where the result is revealed that no significant peaks are observed at the pure LDPE and three significant absorption peaks are observed at different wave numbers where bending and stretching absorptions are attributed to the C-H and -CH₂ compounds, respectively.

Thermal stability is also studied by TG/DTG analysis. The initial degradation temperature of pure LDPE is very low and it shifted to higher order by the addition of RGO. Initially the decomposition was very low due to the presence of moisture content and after a certain temperature the pure LDPE is totally burned but the RGO loaded LDPE nanocomposites are lost at different amount. Hence the nanocomposites are more stable than pure LDPE in thermal applications.

In mechanical analysis, the ultimate tensile strength (UTS), elongation at break and Young modulus are also studied. An anomalous result is revealed for one sample which may be due to the improper dispersion of RGO. Elongation at break and Young modulus are also revealed as increasing value with the further incorporation of RGO. All of the results exhibited that the mechanical strength of the nanocomposite is better than that of pure LDPE.

The electrical analysis of any composite is very critical. In this analysis current density, conductivity and dielectric properties are studied. The current density verses voltage at different temperature are revealed that the current density is very low at room temperature and it is increased with the increase of temperature, which is very consistent with the semiconducting nature of materials. In ac analysis, the results also revealed that the good dielectric constant, low dielectric loss factor are the essential properties of dielectric material. The frequency dependent electrical conductivity is increased with the increase of frequency but decreased with the increase of RGO concentration. This decreasing of conductivity maybe due to the coagulation of foreign particle in higher wt% which introduce deep traps inside the material and reduced the mobility of charge careers.

5.2 Recommendations for Future Work

To investigate further information about the composite, the following work should be done:

- ❖ Injection molding machine will be fabricated to prepare the same composite to investigate the variation of their result.
- ❖ Carbon nanotube will be incorporated instead of graphene with the LDPE.

- ❖ The surface morphology will be observed using transmission electron microscopy (TEM).
- ❖ It will be tried to fabricated biodegradable and ecofriendly plastic instead of polyethylene to save our environment.

5.3 References

- [1] Vantadori S., Carpinteri A., and Zanichelli A., “Lightweight construction materials: Mortar reinforced with date-palm mesh fibres”, *Theoretical and Applied Fracture Mechanics*, Vol. 100, pp. 39–45, 2019.
- [2] Gaska K., Xu X., Gubanski S., and Kádár R., “Electrical, Mechanical, and Thermal Properties of LDPE Graphene Nanoplatelets Composites Produced by Means of Melt Extrusion Process”, *Polymer*, Vol. 9, pp. 1–12, 2017.
- [3] Michael F. Hochella, Jr., “There’s plenty of room at the bottom: Nanoscience in geochemistry”, *Geochimica et Cosmochimica Acta*, Vol. 66, No. 5, pp. 735–743, 2002.
- [4] D.L. Chung D., “Engineering Materials and Processes”, Springer, 2nd Edition, chap. 1, pp. 8-26, 2009.
- [5] Rosi G.F., Frechette M., David E., and Fabiani D., “Behavior of Polyethylene-Based Nanocomposites Containing Multi-layer Graphene Filler”, University of Bologna, Bo, Italy, pp. 473–476, IEEE, 2017.
- [6] Gupta B., Kumar N., Panda K., Kanan V., Joshi S. and Fisher I. V., “Role of oxygen functional groups in reduced graphene oxide for lubrication”, *Nature Scientific Reports*, Vol. 7:45030, pp. 1–14, 2017.
- [7] Sabet M., Soleimani H., “Inclusion of graphene on LDPE properties”, *Heliyon*, Vol. 5, pp. 1–10. 2019.
- [8] Bu J., Huang X., Li S., Jiang P., “Significantly enhancing the thermal oxidative stability while remaining the excellent electrical insulating property of low density polyethylene by addition of antioxidant functionalized graphene oxide”, *Carbon*, Vol. 106, pp. 218–227, 2016.

- [9] Fahim I. S., Mamdouh W., Salem H. G., “Effect of Processing Technique on LDPE Thin Films and sheets”, *International Journal of Engineering Inventions*, Vol. 4, pp. 01-05, 2015.
- [10] Baeurle S. A., “Multiscale modeling of polymer materials using field-theoretic methodologies: a survey about recent developments”, *Journal of Mathematical Chemistry*, Vol. 46, pp. 363–426, 2009.
- [11] Tomar S., Singh L., and Sharma V., “Miraculous adjuvants: The pharmaceutical polymers”, *Internal Research Journal of Pharmacy*, Vol. 7(7), pp. 10-18, 2016.
- [12] Gad Y. H., Magida M. M., and El-Nahas H. H., “Effect of ionizing irradiation on the thermal blend of waste low density polyethylene/ethylene vinyl acetate/bitumen for some industrial applications”, *Journal of Industrial and Engineering Chemistry*, Vol. 16, pp. 1019–1024, 2010.
- [13] Marashdeh W. F., Longun J., and Iroh. J. O., “Relaxation behavior and activation energy of relaxation for polyimide and polyimide–graphene nanocomposite”, *Journal of Applied Polymer Science.*, Vol. 133, pp. 1-8, 2016.
- [14] Geim A. K., Novoselov K. S., “The Rise of Graphene”, *Nature Materials*, Vol. 6, pp. 183-191, 2007.
- [15] Marcano D. C., Kosynkin D. V., Berlin J. M., Sinitskii A., Sun Z, Slesarev A., Alemany L. B., Lu W., and Tour J. M., “Improved Synthesis of Graphene Oxide”, *ACS Nano*, Vol. 4, pp. 4806-4814, 2010.
- [16] Ho K. I., Boutchich M., Su C.Y., Moreddu R., Marianathan E.S.R., Montes L., and Lai C.S., “A self-aligned high-mobility graphene transistor: decoupling the channel with fluorographene to reduce scattering”, *Advanced Material*, Vol. 27, pp. 6519–6525, 2015.
- [17] Lee C., Wei X., Kysar J. W., and Hone J., “Measurement of the elastic properties and intrinsic strength of monolayer graphene”, *Science*, Vol. 321, pp. 385-388, 2008.
- [18] Balandin A. A., Ghosh S., Bao W., Calizo I, Teweldebrhan D., Miao F., and Lau C.N., “Superior thermal conductivity of single-layer graphene”, *Nano Letter.*, Vol. 8, pp. 902-907, 2008.

- [19] Novoselov K. S., Geim A. K., Morozov S. V., Jiang D., Zhang Y., Dubonos S. V., Grigorieva I. V., and Firsov A. A., “Electric field effect in atomically thin carbon films”, *Science*, Vol. 306 (5696), pp. 666-669, 2004.
- [20] Dresselhaus M. S., Araujo P. T., “Perspectives on the 2010 Nobel Prize in Physics for Graphene”, *ACS Nano*, Vol. 4, NO. 11, pp. 6297–6302, 2010.
- [21] Cooper D. R., D’Anjou B., Ghattamaneni N., Harack B., Hilke M., Horth A., Majlis N., Massicotte M., Vandsburger L., Whiteway E., and Yu V., “Experimental review of graphene”, *ISRN Condensed Matter Physics*, Vol. 2012, pp. 1-56, 2012.
- [22] Charlier J. C., Eklund P. C., Zhu J., and Ferrari A. C., “Electron and Phonon Properties of Graphene: Their Relationship with Carbon Nanotubes”, *Topics in applied physics*, Vol. 111, pp. 673–709, 2008.
- [23] Novoselov K. S., Geim A. K., Morozov S. V., Jiang D., Katsnelson M. I., Grigorieva I. V., Dubonos S. V., and Firsov A. A., “Two-dimensional gas of massless Dirac fermions in graphene”, *Nature*, Vol 438, pp. 197-200, 2005.
- [24] Chen J. H., Jang C., Xiao S., Ishigami M., and Fuhrer M. S., “Intrinsic and extrinsic performance limits of graphene devices on SiO₂”, *Nature Nanotechnology*, Vol. 3, pp. 206-209, 2008.
- [25] Morozov S. V., Novoselov K. S., Katsnelson M. I., Schedin F., Elias D. C., Jaszczak J. A., and Geim A. K., “Giant intrinsic carrier mobilities in graphene and its bilayer”, *Physical Review Letters*, Vol. 100, pp. 016602(1-4), 2008.
- [26] Los J. H., Zakharchenko K. V., Katsnelson M. I., and Fasolino A., “Melting temperature of graphene”, *Physical Review B*, Vol. 91, pp. 045415(1-6), 2015.
- [27] Zhong M., Xu D., Yu X., Huang K., Liu X., Qu Y., Xu Y., Yang D., “Interface coupling in graphene/fluorographene heterostructure for high-performance graphene/silicon solar cells”, *Nano Energy*, Vol. 28, pp. 12–18, 2016.
- [28] Akinwande D., Tao L., Yu Q., Lou X., Peng P., and Kuzum D., “Large-area graphene electrodes”, *IEEE Nanotechnology Magazine*, pp. 6-14, September 2015.

- [29] Yang W., Ni M., Ren X., Tian Y., Li N., Su Y., and Zhang X., “Graphene in supercapacitor applications”, *Current Opinion in Colloid & Interface Science*, Vol. 20, pp. 416–428, 2015.
- [30] Ma C., Wang X., Ma Y., Sheng J., Li Y., Li S., and Shi J., “Carbon nanofiber/graphene composite paper for flexible supercapacitors with high volumetric capacitance”, *Materials Letters*, Vol. 145, pp. 197-200, 2015.
- [31] Batignani G., Bettarini S., Borghi G., Boscardin M., Ciarrocchi A., Crivellari M., Coletti C., Gaspare A. D., Lieto A. D., Forti F., Goretti D., Mishra N.P., Paoloni E., Rizzo G., Scherzinger J., Tredicucci A., Vicarelli L., and Zorzi N., “Development of graphene-based ionizing radiation sensors”, *Nuclear Instruments and Methods in Physics Research A*, Vol. 936, pp. 666-668, 2018.
- [32] Chen S., Ma W., Xiang H., Cheng Y., Yang S., Weng W., and Zhu M., “Conductive, tough, hydrophilic poly(vinyl alcohol)/graphene hybrid fibers for wearable supercapacitors”, *Journal of Power Sources*, Vol. 319, pp. 271-280, 2016.
- [33] Kumar K. and Yadav B. C., “An Overview on the Importance of Chemical Vapour Deposition Technique for Graphene Synthesis”, *Advanced Science, Engineering and Medicine*, Vol. 10, pp. 1–4, 2018.
- [34] Tanahashi M., “Development of fabrication methods of filler/polymer nanocomposites: With focus on simple melt-compounding-based approach without surface modification of nanofillers”, *Materials*, Vol. 3, pp. 1593-1619, 2010.
- [35] Rauwendaal C., “Polymer Extrusion 5E”, chap. 1, pp. 6, Hanser Publishers, Munich; Hanser Publications, Cincinnati, 2013.
- [36] Fadeyibi A., Osunde Z. D., Agidi G. and Egwim E. C., “Design of single screw extruder for homogenizing bulk solids”, *Agricultural Engineering International: CIGR*, Vol. 18(4), pp. 222-231, 2016.
- [37] Chokshi R., Zia H., “Hot-Melt Extrusion Technique: A Review”, *Iranian Journal of Pharmaceutical Research*, Vol. 3, pp. 3-16, 2004.
- [38] Guise O., Strom C., and Preschilla N., “STEM-in-SEM method for morphology analysis of polymer systems”, *Polymer*, Vol. 52, pp. 1278-1285, 2011.

- [39] Wheatcroft L., Ozkaya D., Cookson J., and Inkson B. J., “Towards in-situ TEM for Li-ion battery research”, *Energy Procedia*, Vol. 151, pp. 163-167, 2018.
- [40] Scoutaris N., Vithani K., Slipper I., Chowdhry B., and Douroumis D., “SEM/EDX and confocal Raman microscopy as complementary tools for the characterization of pharmaceutical tablets”, *International Journal of Pharmaceutics*, Vol. 470, pp. 88-98, 2014.
- [41] Stobinski L., Lesiak B., Malolepszy A., Mazurkiewicz M., Mierzwa B., Zemek J., Jiricek P., and Bieloshapka I., “Graphene oxide and reduced graphene oxide studied by the XRD, TEM and electron spectroscopy methods”, *Journal of Electron Spectroscopy and Related Phenomena*, Vol. 195, pp. 145–154, 2014.
- [42] Bekiaris G., Peltre C., Jensen L. S., and Bruun S., “Using FTIR-photoacoustic spectroscopy for phosphorus speciation analysis of biochars”, *Spectrochimica Acta Part A: Molecular and Biomolecular Spectroscopy*, Vol. 168, pp. 29–36, 2016.
- [43] Czajka K. M., “Proximate analysis of coal by micro-TG method”, *Journal of Analytical and Applied Pyrolysis*, Vol. 133, pp. 82-90, 2018.
- [44] Silva R.V., Brito J. D., and Dhir R.K., “Tensile strength behaviour of recycled aggregate concrete”, *Construction and Building Materials*, Vol. 83, pp. 108–118, 2015.
- [45] Häßler W., Rodig C., Damm C., Scheiter J., Schultz L., Aubele A., Sailer B., and Schlenga K., “Increased critical current density of in-situ MgB₂ wires by Mg deficiency”, *Physica C*, Vol. 510, pp. 8–12, 2015.
- [46] Kurek P., Fafilek G., “Comparative two- and four-probe impedance measurements on BICUVOX.10”, *Solid State Ionics*, Vol. 119, pp. 151–158, 1999.
- [47] Manta A., Tserpes K. I., “Numerical computation of electrical conductivity of carbon nanotube-filled polymers”, *Composites Part B*, Vol. 100, pp. 240-246, 2016.
- [48] Chen Q., Wang J., and Zhang Y., “Activation energy study of phosphorus-doped microcrystalline silicon thin films”, *Optik*, Vol. 127, pp. 10437–10441, 2016.

- [49] Lin X., Fan L., Ren D., Jiao Z., Coates P., and Yang W., “Enhanced dielectric properties of immiscible poly (vinylidene fluoride)/low density polyethylene blends by inducing multilayered and orientated structures”, *Composites Part B*, Vol. 114, pp. 58-68, 2017.
- [50] Sharma J., Chand N., and Bapat M.N., “Effect of cenosphere on dielectric properties of low density polyethylene”, *Results in Physics*, Vol. 2, pp. 26–33, 2012.
- [51] Muruganandi G., Saravanan M., Vinitha G., Raj M. B. J. and Girisun T.C. S., “Barium borate nanorod decorated reduced graphene oxide for optical power limiting applications”, *Optical Materials*, Vol. 75, pp. 612–618, 2018.
- [52] Zhang Q., Diao D., and Yang L., “Dangling bond induced cross-linking model in nanoscratched graphene layers”, *Surface and Coatings Technology*, Vol. 237, pp. 230–233, 2013.
- [53] Song Z., Zhu H., Shi W., Sun Dalin., and Ruan S., “Ultrafast charge transfer in graphene-WS₂ Van der Waals heterostructures”, *Optik - International Journal for Light and Electron Optics*, Vol. 174, pp. 62–67, 2018.
- [54] Jin S., Gao Q., Zeng X., Zhang R., Liu K., Shao X., and Jin M., “Effects of reduction methods on the structure and thermal conductivity of free-standing reduced graphene oxide films”, *Diamond & Related Materials*, Vol. 58, pp. 54–61, 2015.
- [55] Latif I. A., Merza S. H., “Fabrication of Functionalize Reduce Graphene Oxide and Its Application in Ampicillin Detection”, *Nanoscience and Nanotechnology*, Vol. 6(2), pp. 24–33, 2016.
- [56] Chen Y., Niu Y., Tian T., Zhang J., Wang Y., Li Y. and Qin L. C., “Microbial reduction of graphene oxide by *Azotobacter chroococcum*”, *Chemical Physics Letters*, Vol. 677, pp. 143–147, 2017.
- [57] Saleem H., Haneef M. and Abbasi H. Y., “Synthesis route of reduced graphene oxide via thermal reduction of chemically exfoliated graphene oxide”, *Materials Chemistry and Physics*, Vol. 204, pp. 1–7, 2018.

- [58] Mahajan C. R. and Mishra S., “Effect of Graphitic Nanomaterials on Thermal, Mechanical and Morphological Properties of Polypropylene Nanocomposites”, *Research & Development in Material science*, Vol. 11(4), pp. 1190–1201, 2019.
- [59] Carotenuto G., Nicola S. D., Ausanio G., Massarotti D., Nicolais L. and Pepe G. P., “Synthesis and characterization of electrically conductive polyethylene-supported graphene films”, *Nanoscale Research Letters*, Vol. 9:475, pp. 1–7, 2014.
- [60] Lei H., Liu Z., He C., Zhang S. C., Liu Y.Q., Hua C. J., Li X. M, Li F., Chen C. M. and Cai R., “Graphene enhanced low-density polyethylene by pretreating and melt compounding”, *Royal Society of Chemistry*, 2016.
- [61] Sirocic A. P., Rescek A., Scetar M., Krehula L. K. and Murgic Z. H., “Development of low density polyethylene nanocomposites films for packaging”, *Polymer Bulletin*, Vol. 71, pp. 705–717, 2014.
- [62] Giuliadori M. J., Lujan H. L., Briggs W. S., Palani G., and DiCarlo S. E., “Hooke’s law: applications of a recurring principle”, *Advances in Physiology Education*, Vol. 33, pp. 293–296, 2009.
- [63] Sabet M., Soleimani H., and Mohammadian E., “Effect of Graphene and Carbon Nanotube on Low-Density Polyethylene Nanocomposites”, *Journal of Vinyl & Additive Technology*, pp. 1–6, 2018.
- [64] Carotenuto G., Nicola S. D., Palomba M., Pullini D., Horsewell A., Hansen T. W. and Nicolais L., “Mechanical properties of low-density polyethylene filled by graphite nanoplatelets”, *Nanotechnology*, Vol. 23, pp. 1–8, 2012.
- [65] Ning N., Li S., Sun H., Wang Y., Liu S., and Yao Y., Yan B., Zhang L., Tian M., “Largely improved electromechanical properties of thermoplastic polyurethane dielectric elastomers by the synergistic effect of polyethylene glycol and partially reduced graphene oxide”, *Composites Science and Technology*, Vol. 142, pp. 311–320, 2017.